STUK-YTO-TR 56

Use of high energy gamma emission tomography for partial defect verification of spent fuel assemblies

Final report on the Task FIN A98 of the Finnish Support Programme to IAEA Safeguards

F. Lévai, S. Dési, M. Tarvainen, R. Arlt

NOVEMBER 1993

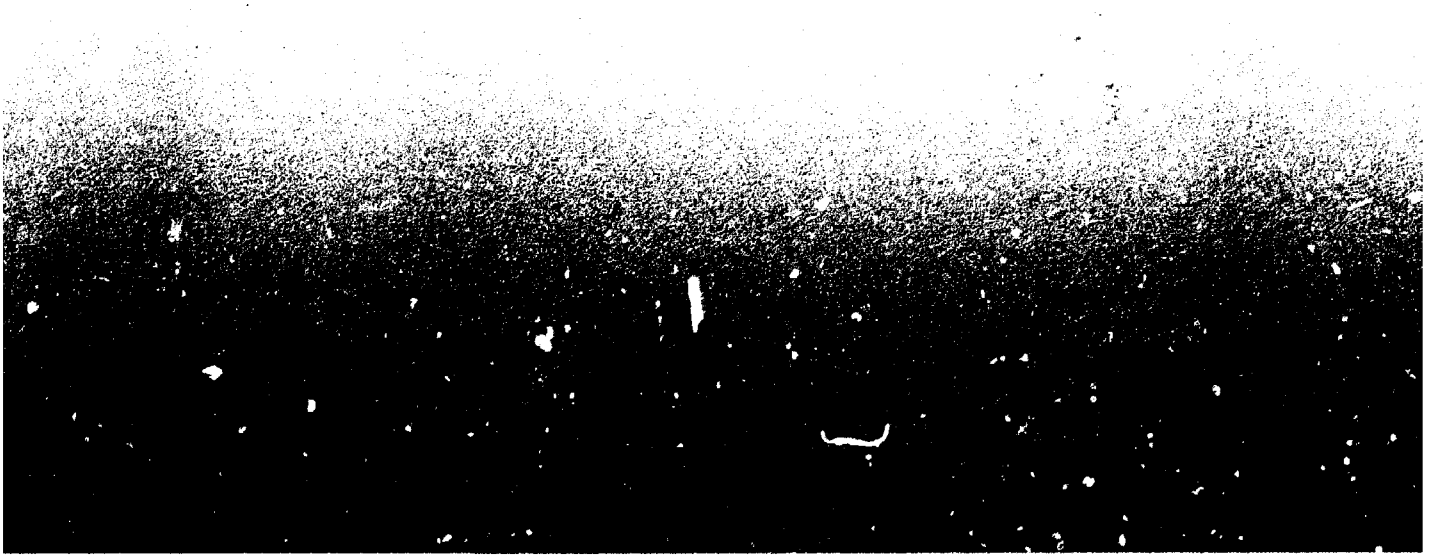

SÄTEILYTURVAKESKUS
Strålsäkerhetscentralen
Finnish Centre for Radiation and Nuclear Safety

STUK-YTO-TR 56
NOVEMBER 1993

Use of high energy gamma emission tomography for partial defect verification of spent fuel assemblies

Final report on the Task FIN A98 of the Finnish Support Programme to IAEA Safeguards

F. Lévai, S. Dési
Technical University of Budapest
Institute of Nuclear Techniques

M. Tarvainen
Finnish Centre for Radiation and Nuclear Safety (STUK)
Department of Nuclear Safety

R. Arlt
International Atomic Energy Agency (IAEA)

FINNISH CENTRE FOR RADIATION AND NUCLEAR SAFETY
P.O.BOX 268, FIN-00101 HELSINKI
Phone +358 0 70821

ISBN 951-47-7975-1
ISSN 0785-9325

Painatuskeskus Oy
Helsinki 1993

LÉVAI, Ferenc, DÉSI, Sándor (Technical University of Budapest), TARVAINEN, Matti (Finnish Centre for Radiation and Nuclear Safety, STUK), ARLT, Rolf (International Atomic Energy Agency, IAEA). Use of high energy gamma emission tomography for partial defect verification of spent fuel assemblies. Final report on the Task FIN A98 of the Finnish Support Programme to IAEA Safeguards. STUK-YTO-TR 56. Helsinki 1993. 51 pp.

ISBN 951-47-7975-4
ISSN 0785-9325

Keywords: Safeguards, spent fuel, NDA, partial defect testing, tomography

ABSTRACT

The possibility to use passive gamma emission tomography for revealing non-destructively the rod structure of spent BWR fuel assemblies has been studied in cooperation with the Finnish Support Programme to the IAEA Safeguards (task FIN A98) and the Technical University of Budapest in Hungary. The ultimate goal is to develop partial defect verification methods for verification of spent nuclear fuel. The task included experimental measurements of irradiated BWR assemblies using underwater measurement techniques together with computer analysis of the measured data as well as computer simulation of tomographic measurements. The results obtained show that rod-level partial defect verification of spent LWR fuel assemblies is feasible using computed gamma emission tomography. This report describes the results of this project.

CONTENS

1 INTRODUCTION

According to the Safeguards Criteria of the IAEA, partial defect verification of spent Light Water Reactor (LWR) fuel is needed in certain cases e.g. in case of conclusive negative surveillance. According to present criteria, partial defect verification of spent fuel assemblies is required to reveal missing of more than 50 % of the nuclear material (rods) or replacement them e.g. by dummies. The 50 % limit reflects the state of the art of the partial defect verification methods available.

Verification of the number of fuel rods may be needed also in reprocessing plants before the identity of the fuel assemblies is lost by cutting and dissolving the rods. It is also possible that partial defect verification will be required prior to the final disposal of spent fuel, if feasible methods are available. At the moment, there is not, however, a practical non-destructive (NDA) method available that could be used for partial defect verification of LWR fuel or that could reveal the presence of individual rods.

More or less all of the "integral" methods used at the moment measure the fuel assembly as one entity and their potential for partial defect testing is limited. Therefore an alternative "differential" measurement approach, where information is explicitly obtained from each fuel rod, may be essential.

A method based on non-destructive tomographic verification is very powerful to map the rod structure of a spent fuel assembly and to reveal missing or dummy rods. In order to get information of the inner rods of a fuel assembly, highly penetrating gamma rays or neutrons need to be used.

2 BASIC PRINCIPLES

A non-destructive section imaging technique reconstructs an image from the measured radiation intensity profiles of the object. During measurement, the intensity at selected directions of the object is detected. Measurements are made systematically by a scanning process. A series of measured intensities at a certain angle is called a projection or a view.

The origin of the measured radiation can be the radioactivity emitted by the object (emission imaging). Secondary radiation induced by an external interrogating source (induced emission imaging) may be detected as well as the radiation transmitted through the object (transmission imaging).

A mathematical program is used to calculate the section image from measured projections.

In the case of transmission imaging, the measured values are line integrals of the attenuation coefficients. This type of calculations are well developed and extensively used in medical X-ray imaging. The mathematical equations are linear and can contain convenient image processing techniques.

The mathematics and the methods of the emission imaging differ somewhat from the transmission imaging. The mathematical equations are highly nonlinear and complex. The development of mathematical methods is a rapidly growing field; however, there are no algorithms available for practical use of emission imaging in a strongly absorbing media like nuclear fuel material.

3 SECTION IMAGING OF SPENT FUEL ASSEMBLIES

Gamma ray measurements are made from the side of an irradiated fuel assembly that is partially raised from the storage rack or moved to a measurement position. A gamma detector provides a response that is just a relative number. The magnitude of the number depends in part on the burnup and the cooling time of the assembly. Figure 1 illustrates different approaches to the section imagining of spent fuel in cases where one fuel rod is missing (left) or the array of 8 x 8 rods is full (right).

3.1 Integral measurement with reference data

In this mode quantitative measurements of gamma signals are performed and reference data/calibration curves are used for the evaluation. This is the case of Figure 1 a). The most that might be expected from a single set of such measurements is a consistency check of the operator declared exposures and cooling times.

Another difficulty lies in the fact, that fission products may not be uniformly distributed axially and radially within a fuel assembly. The local (rod-to-rod) power distribution can vary because of the location of burnable poison rods and control rods, location in the core, initial enrichment and configuration of the assembly. A minor factor is a possible axial and radial migration of fission products within individual fuel rods.

The sensitivity of this method to detect missing of irradiated fuel rods is very low. This is due mainly to the uncertainty of reference data and due to the self absorption of gamma rays inside the assembly, even in the case of detecting high energy fission product gammas.

3.2 Scanning and reference data

Measuring emerging radiation in parallel strips at one or more radial orientations provides a higher sensitivity to detect the removal of irradiated rods than that obtained in the case of an integral measurement. The difficulty with reference data, however, remains the same. Figure 1 b) shows the principle of such a measurement.

3.3 Full scanning and image reconstruction

By scanning the assembly with a regular pattern at several orientations, a data set is obtained that is suitable for calculation of a section image. This process results in an activity map of the detected gamma radiation across the layer scanned. This is illustrated by Figure 1 c). The image gives a rod-to-rod distribution of the concentration of the gamma emitters. The high sensitivity of this approach to detect removal of irradiated rods is explained by the following facts:

- There is no need for a reference data set because the activity map provides an inherent rod-to-rod comparison of fission product gamma activities.
- The effect of a single missing rod is very low in the scanning data at one orientation (usually lower than the noise level). The image reconstruction process uses all the scanning data for calculating each image point. Noise, i.e. statistical fluctuations in different scans are uncorrelated and the averaging effect improves the signal-to-noise ratio by increasing signals and decreasing noise.

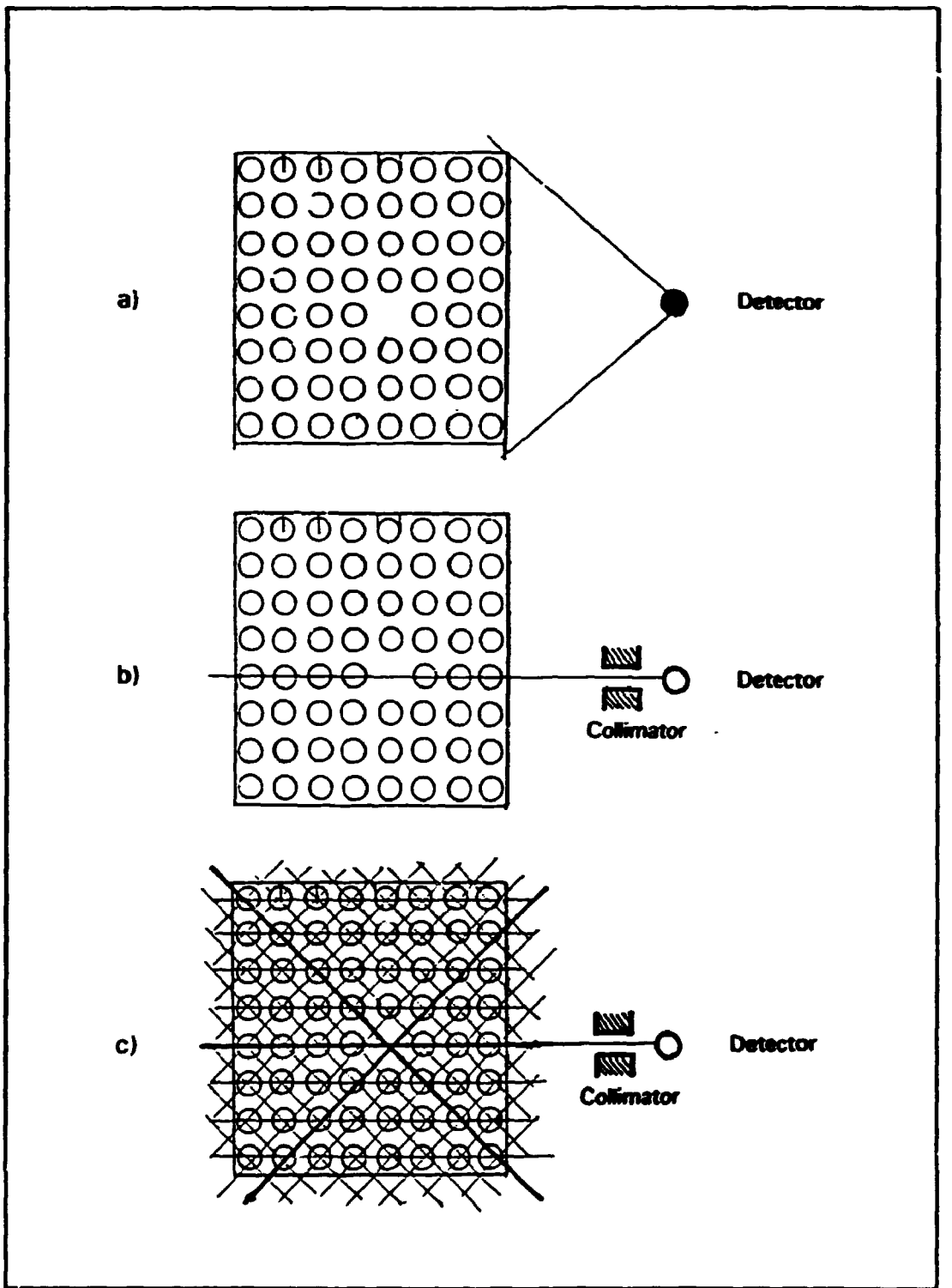

Figure 1. Effect of a missing fuel rod on the measured count rate of an 8 x 8 array in three different measurement approaches. a) In an integral measurement the effect is negligible; b) in a differential (scanning) measurement the effect is still small; c) in full scanning and image reconstruction the effect can be well above the noise level.

4 EXPERIMENTAL ARRANGEMENT

4.1 Scanning procedure

A single detector system with mechanical movement of the detector is shown in Figure 2. The fuel assembly is fixed while the detection system is moving at a certain orientation along a line. When measurement of a projection (view) is finished, the fuel assembly is rotated and another view is scanned.

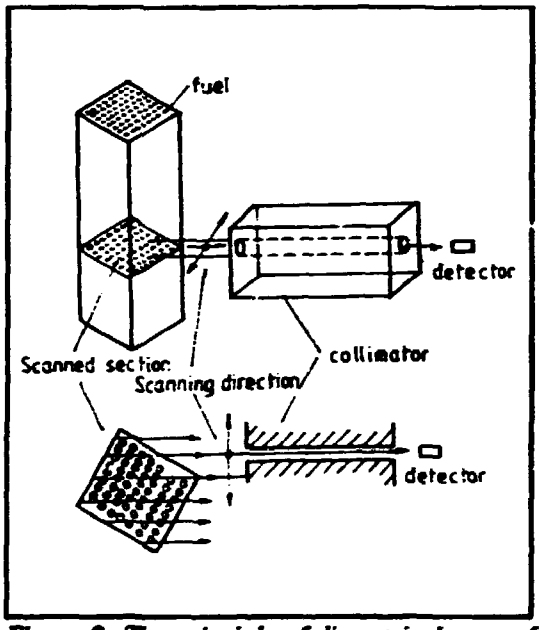

Figure 2. The principle of diametrical scan of a fuel assembly.

4.2 Detectors for high energy gamma rays

For tomographic verification of spent fuel assemblies the measurements are carried out by detecting the gamma radiation emitted by the fission products. Because of the high gamma absorption coefficient of the fuel material, the high energy gamma rays should be measured in order to keep the self absorption of radiation coming from the inner parts of the assemblies at a minimum. So, the fission products which should be detected are ^{144}Pr (E_γ = 2186 keV and 1489 keV) and ^{154}Eu (E_γ = 1275 keV).

The detected high energy gamma rays must be separated from other, low energy and usually much higher intensity gamma rays emitted mainly by the isotopes ^{137}Cs (E_γ = 662 keV) and ^{134}Cs (E_γ = 796 and 605 keV). Consequently, energy-selective detectors should be used taking into account the special requirements of a short measurement time and the portability of the instrument.

To fulfill these requirements, a system consisting of small-sized energy-selective detectors combined with a suitable gamma collimator to ensure sufficient directional sensitivity is used. These requirements determine also the size and weight of the collimator. To keep them as low as possible, the detector dimensions should not exceed a few millimeters. To meet these requirements only small-sized room temperature semiconductor detectors operating in pulse mode can be considered. Because the fraction of photoelectric effect in these detectors at high gamma ray energies is very small, only pulses originating from the Compton interaction can be used. The amplitude distribution of pulses originating from Compton interactions is proportional to the gamma energies in question. This is why it is possible to separate the part of the Compton spectrum that belongs to the highest energy gamma rays from those belonging to the lower energy gamma rays using an amplitude discriminator. It allows to

count pulses with greater amplitudes than the Compton edge of the highest background radiation. This level is about 478 keV for ^{137}Cs.

For this purpose detectors of low atomic numbers, such as Si, Si(Li) as well as other recently developed room temperature detectors with higher Z, like CdTe and HgI_2, can be used.

To ensure the higher energy Compton electrons to deposit all their energy within the detector, the size of the detector should be large enough. The smallest dimension of the detector should be equal or larger than the range of the Compton edge electrons belonging to the lowest energy gamma radiation to be detected. This means the range of electrons of about 1 MeV for ^{154}Eu.

Depending on the activity of the assemblies measured, the sensitivity of the system can be easily adjusted by changing the volume (area) of the detector in order to avoid overloading problems.

The requirements concerning the detector resolution (noise) are not so strict because the broad Compton spectrum is not significantly altered by the energy resolution of the detector and the discrimination level is above the electronic noise. As a result, detectors with moderate energy resolution can be used. For the actual measurements two main room temperature detector types have been tested, Si(Li) detectors and CdTe detectors.

4.2.1 Si(Li) detectors

Lithium drifted silicon detectors of two different sizes have been used. The detectors were made by Microvacuum Ltd, Budapest, Hungary. The larger ones had a sensitive thickness of 1,5 mm and a diameter of 16 mm. The smaller ones were 2 mm thick with a diameter of 4 mm (see Fig. 7 a), page 15). These detectors have been tested in a single detector measuring system and they proved to be quite reliable in a wide range of gamma irradiation rates /1/. The energy resolution (noise line width) of these detectors was 25 keV and 15 keV FWHM, respectively.

4.2.2 CdTe detectors

The use of the relatively new high-Z CdTe detectors offers some advantages. The probability of Compton interaction, proportional to the density of the detector material, is more than twice of that of silicon. Furthermore, the range of Compton electrons in CdTe is only about one third of that in silicon. To have the same detection efficiency, a significantly smaller volume CdTe detector is needed. In this work the minimum sensitive thickness of the detector is less than 1 mm and the sensitive volume is only about 50% of an equivalent silicon detector.

The decreased detector size makes it possible to use smaller collimators which in turn decreases the size and weight of the whole measurement head. In the multidetector measurement system, ten square-shaped, 10 mm x 10 mm CdTe detectors with a sensitive thickness of 1 mm were used (see Fig. 7 b), page 15). The detectors were made by Eurorad, Strasbourg, France or by the Riga Scientific Research Institute for Radioisotope Apparatus, Riga, Latvian Republic. The sensitivity of these detectors was about the same as that of the larger Si(Li) detector and the electronic noise was less than 15 keV FWHM. The scatter of sensitivity among the ten detectors was found to be less than $\pm$ 5 % during a ^{60}Co gamma irradiation (integral count rate above the noise level).

4.3 Polarization

The stability of silicon detectors is good. No shift or change in the sensitivity has been detected during the measurement period even at the highest gamma irradiation rates.

With the recommended detector bias of the CdTe detectors, however, a slow change in

sensitivity i.e. decrease of the pulse amplitude has been detected. The extend of this change varied between 2,5 % - 40 % depending on the gamma dose rate during the measurement. The time needed for stabilization of the detectors varied from minimum 30 minutes to 2 hours. This phenomenon is known as polarization under radiation and it is caused mainly by deep-lying acceptors (electron traps) in the space-charge region of the detector.

The filling-up of these traps with electrons depends strongly on the drift velocity of electrons which, on the other hand, is controlled by the electric field intensity inside the detector i.e. the detector bias. This is why it was reasonable to suppose that this kind of polarization could be considerably decreased by applying higher detector bias. So, the detector bias was increased by about 60 % which eliminated the polarization even with the ^{60}Co gamma irradiation rates of around 150 R/h which is equivalent to the measurement conditions with the most active fuel assemblies. As a consequence of the higher detector bias, the electronic noise increased about 50 % which is tolerable in this case. The question, how the magnitude of the polarization and its elimination depend on the raw material of the CdTe detectors and on the manufacturing process remains to be answered.

4.4 Signal processing electronics

At the very high gamma dose rates of the tomographic measurements, handling of a large number of pulses, up to several millions per second, is required. For this purpose a fast pulse shaping and processing electronics has been developed. The block diagram is shown in Figure 3.

The detector (D) pulses are fed into a fast rise time charge sensitive preamplifier (P.A.) with a pulse handling capability up to 2 x 10^6 MeV/s. The preamplifier pulses are then shaped with a delay line and amplified by a fast amplifier A. Pulses are next led to the level discriminator L.D. which passes through pulses above the discriminator level with a rate proportional to the amplitude. These pulses are next converted to a fluctuating D.C. level by a dead-time free AC/DC converter-ratemeter and finally integrated (I) over the desired measuring time. So, a quasi D.C. level appears at the output, which can be transmitted noise-free to a 20 m long underwater cable for evaluation in the noisy environment.

The whole system can process more than 2 x 10^6 pulses per second. Each detector has its own signal processing chain. Each channel may have more than one discriminator level (L.D.).

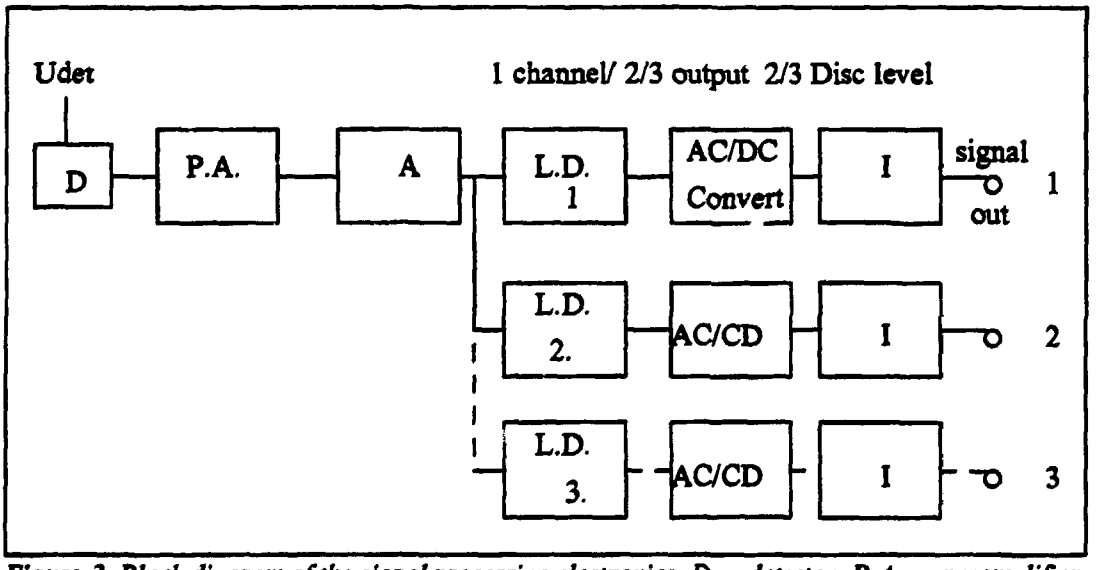

Figure 3. Block diagram of the signal processing electronics. D = detector, P.A. = preamplifier, A = fast amplifier, L.D. = level discriminator, AC/DC = ratemeter and I = integrator.

Each output corresponds to the signal above the amplitude/energy threshold level.

4.5 Directional characteristics

Directional sensitivity of the system has a nearly Gaussian shape which can be described by one parameter, namely FWHM. It depends on the energy of the radiation. The FWHM values with ^{60}Co have measured to be 1° - 1,5° with both detector types.

4.6 Underwater detector head

Figure 4 shows schematically the inner parts of the watertight measurement chamber. It contains the detection system and collimator on a rail for linear movement with a stepping motor. All movements are remote controlled. Only the signal processing unit is inside the detector head under a high radiation field. The fixed detector/collimator measurement geometry is important, because it determines the geometrical resolution of the detection system.

4.7 Control electronics

Control electronics are shown schematically in Figure 5. All the other parts, except the preamplifier/discriminator/ratemeter system (inside the head), are commercially available standard units. The system is controlled by a program run on a 33 MHz Toshiba 6400 laptop computer. All discriminator levels are remote controlled and displayed on the screen during measurement. The whole electronics system is portable and consists of 3 units: A laptop computer, a bus extension unit and a motor driver unit (see Figure 6).

4.8 Principle of multidetector scanning

The first scanning arrangement /2/ used a single detector system moved mechanically for measuring different projections. Although this system worked well, there was a need to decrease the measurement time by a factor of 5 - 6. For measuring a BWR assembly, a length of 200 mm needs to be scanned. With steps of 2 mm, this means 101 measurement points at one view. When 48 views need to be measured, a total of 101 x 48 points should be measured. With measurement time of 2 s per point, the total measurement time using a single detector is about 2,7 hours. The total measurement time requires additional 2,5 hours for mechanical movement of the detector system.

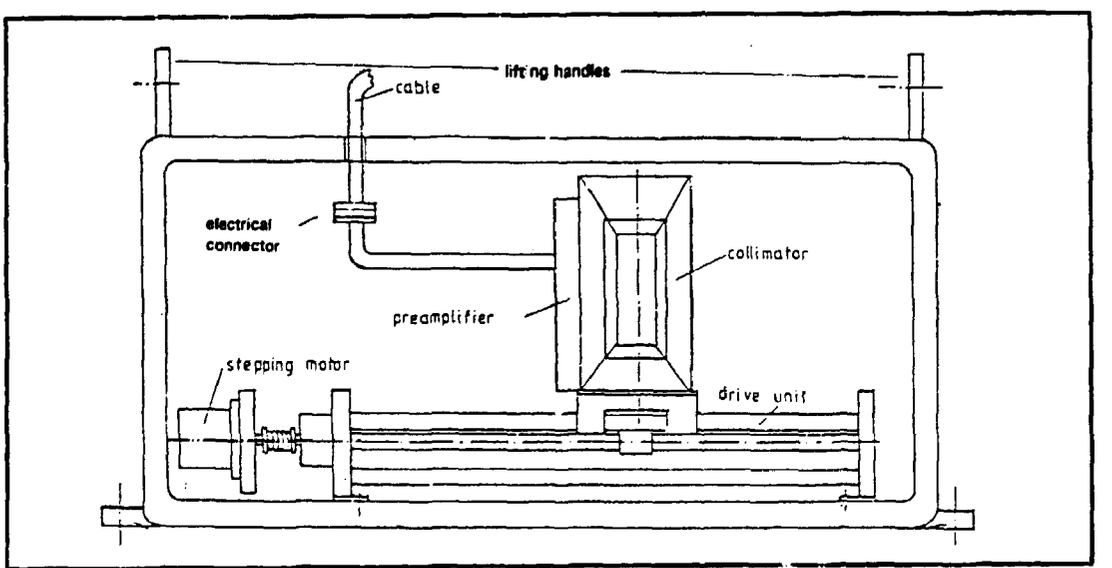

Figure 4. A line drawing of the inner parts of the underwater measurement head used for tomography.

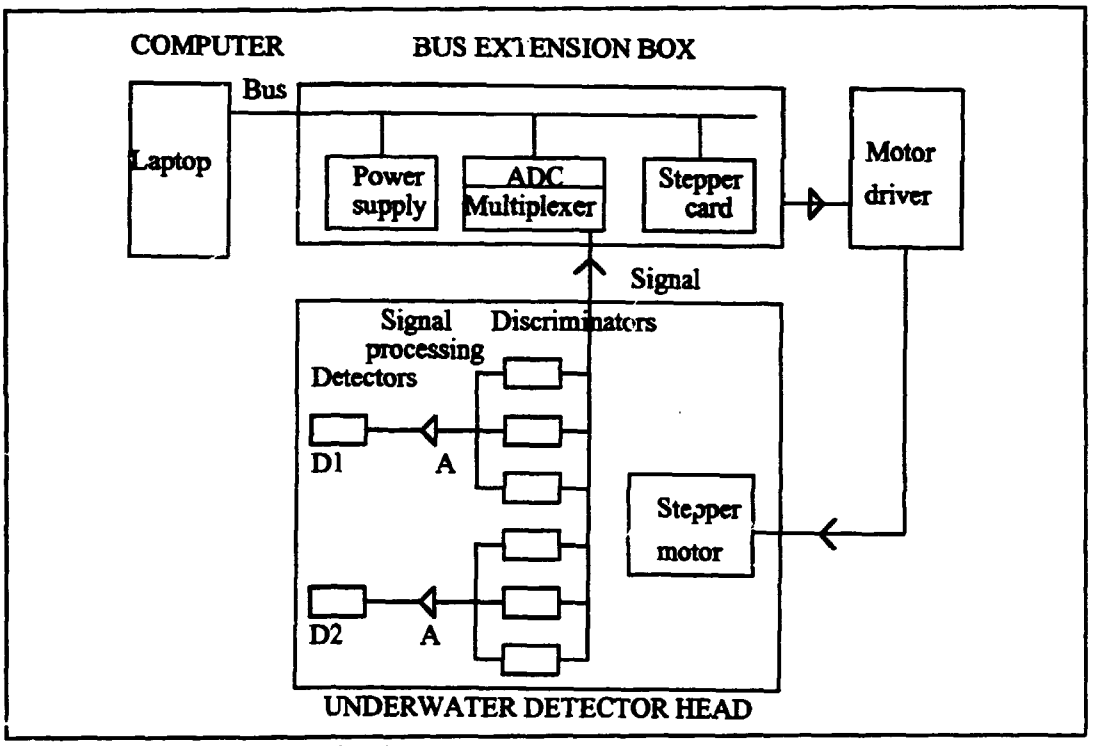

Figure 5. Block diagram of the electronic system.

Figure 6. Control electronics used during the tomographic measurements. The computer (right) controls the whole measurement system. The bus extension box and the stepping motor driver unit (left) include all the measurement electronics needed outside the measurement head.

In principle, an array of detectors that is large enough to cover one side of the assembly by steps of 2 mm would eliminate the need for linear mechanical movement of the detectors. Such a system would measure 48 views in a total measurement time of about 100 seconds not including the time needed to rotate the assembly. In such a case an array of about 100 closely packed thin detectors would be needed.

Mainly for economical reasons an array of 10 CdTe detectors was used. This system measures simultaneously 10 points. The scanning procedure is automatic and remote controlled by a computer. A manual rotation of the assembly by steps of 7,5° is done between successive scans. The detector array is moved in steps of 20 mm between measurements which means that each point is measured once and only by one detector. Scanning of one side (318 mm) requires 15 steps resulting in a measurement time of about 1 minute per side. The total measurement time for 48 views of a BWR assembly takes thus ≤ 1 hour including manual rotation.

Figure 7 a) shows the geometry of the Si(Li) detectors used and Figure 7 b) the geometry of the array of 10 CdTe detectors, respectively.

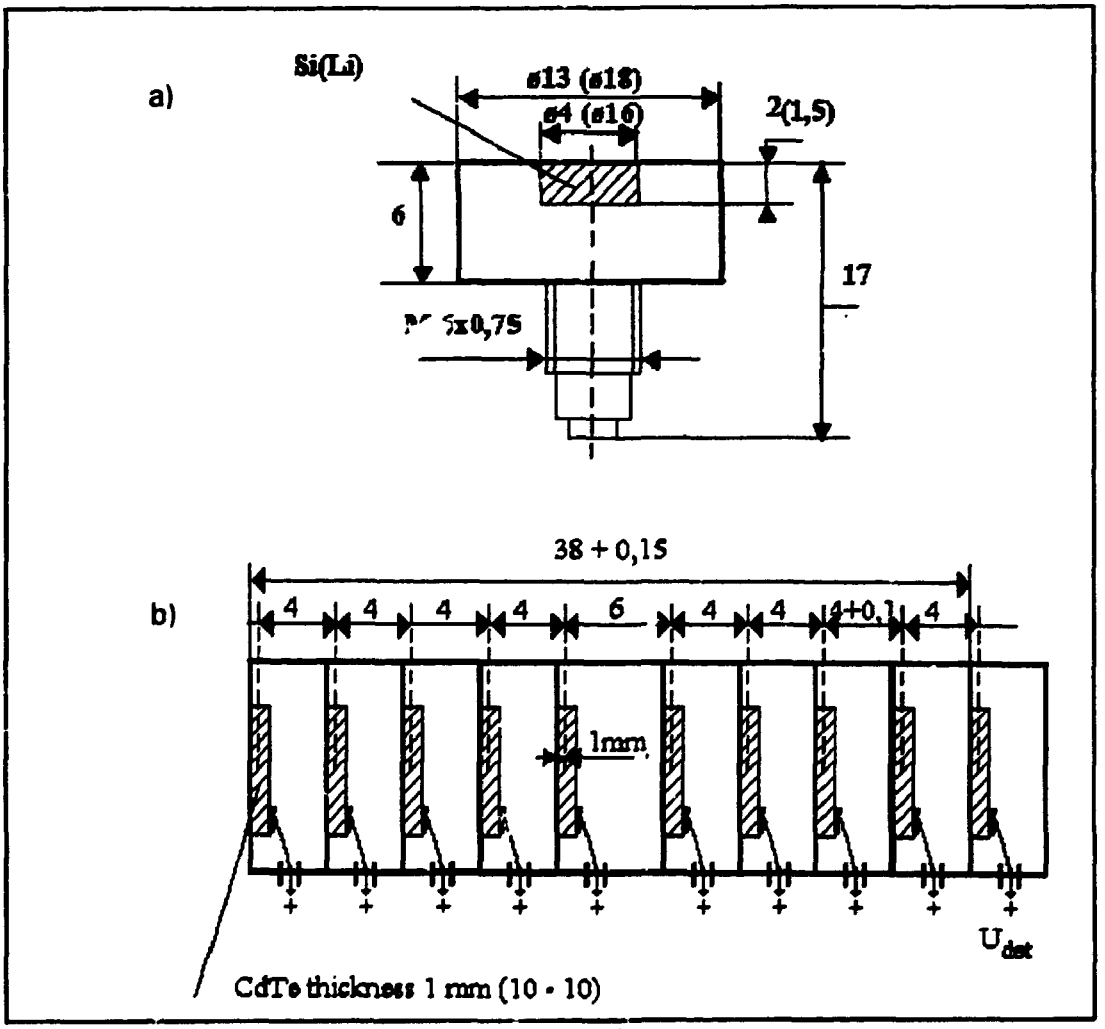

Figure 7. Geometries of the detectors used for tomographic measurements. a) Si(Li) detectors; diameters in parenthesis relate to the smaller sized model and those without parenthesis to the larger model. b) Dimensions of the array of 10 CdTe detectors.

4.8.1 Calibration of detectors

Computer simulation was used to study the influence of sensitivity differences between the 10 CdTe detectors used in the array. It was noticed that sensitivity differences within ± 5 % still make it possible to detect missing of one single fuel rod in the cross section image of ^{154}Eu activity reconstructed from scanned 48 views of a BWR assembly.

Laboratory calibration of detectors was difficult because high energy gamma sources (^{144}Pr and ^{154}Eu) were not available. An on-site calibration procedure at the facility was made in the following way. One flat side of a fuel assembly was scanned by the array in such a way that the same scanning positions were measured by all the detectors. Comparison of readings of different detectors resulted in the calibration factors. They can be used by the software for normalization during image reconstruction. Calibration is needed for each discriminator level i.e. for each detected gamma ray energy. The data can be stored which eliminates the need for recalibration in routine use.

4.8.2 Scanning files

Measurement readings are stored separately for each detector. Scanning file for each measured point is constructed from the stored detector readings by an automatic sub-program. File construction takes into account also the stored calibration factors and different offset values of the electronic units.

5 IMAGE CALCULATION

5.1 Basic mathematical algorithms

Two basic types of mathematical algorithms, an analytic one and an iterative one, have been studied in this work in detail for section imaging of spent fuel assemblies. For the first experimental results, iterative unfolding methods provided promising features /1/. The inaccuracy of the geometrical parameter in practical measurements and the inhomogeneity among the fuel rod activities resulted in increase of the required number of measured views. For a large number of views an analytic type of algorithm is more stable and easier to control. Using *a priori* knowledge of the structure of the fuel type to be measured, a modified model based analytic algorithm was found to be the most suitable for practical use.

5.2 Model based image reconstruction

Basic modules of the technique are the fuel simulation programme and the attenuation compensation programme.

5.2.1 Fuel simulation

Fuel simulation programme calculates expected projections of an arbitrary fuel model. The input of the programme consists of the geometry of the assembly (diameter and total number of rods, their center-to-center distance), activity and attenuation coefficient map of the assembly including statistical distribution of both parameters, detector characteristics (distance and FWHM) with Poisson noise added to the measured signal, position of the center-of-mass as well as the axis of rotation of the assembly.

5.2.2 Attenuation compensation

Absorption coefficient of the fuel material at the detected gamma ray energy is considered to be known in advance (*a priori* knowledge). Detector FWHM value is also necessary to be known at the same energy.

Projections are calculated by the simulation program using these values as $S_\mu(x, \varphi)$ where μ is the linear absorption coefficient, x is the liner distance and φ is the rotational angle. The values used are $\mu(Pr) = 0{,}5\ cm^{-1}$ and $\mu(Eu) = 0{,}65^{-1}$. Projections are calculated for the same case also with a lower absorption value $\mu_o < \mu$ as $S_{\mu o}(x, \varphi)$. Compensation is made in the following way:

$$S_{comp}(x,\varphi) = S_\mu(x,\varphi)\frac{S_{\mu 0}(x,\varphi)}{S_\mu(x,\varphi)} \qquad (1)$$

where $S_\mu(x, \varphi)$ is a projection based on the measurements.

In practice it is not useful to let $\mu_o \rightarrow 0$ because this would emphasize the activity inhomogeneity of fuel rods and the relative decrease caused by a missing rod would become smaller. The best value is $\mu/\mu_o \simeq 2 \div 3$ which provides a large gain. The effect of absorption is, however, only decreased but not fully compensated.

Attenuation compensation has been studied using mathematical simulation. The results show that for a nearly homogeneous fuel rod activity distribution, compensation can be

perfect but care should be taken with strong inhomogeneities among fuel rods.

5.3 Deconvolution

In case of a large FWHM of the detector together with unwanted scattering in the water, separate fuel rods can not be resolved by side scanning. A deconvolution technique can be used to improve detector characteristics and to decrease the smearing effect caused by scattering. This technique needs fine sampling and decreased signal-to-noise ratio. Therefore selection of appropriate detector characteristics is of crucial importance.

5.4 Convolution-backprojection analytic image reconstruction

This program is very similar to the ones well developed for medical applications. The main difference is its flexibility and universality for selecting parameters and applicability for a wide range of problems. This program has been extensively tested by mathematical simulation /1/. It revealed the following important features for imaging fuel assemblies:

- Well resolved side projections can provide gross but not resolved fuel rod structure. Side projection are not very sensitive to a missing rod. In a former feasibility study four measured side projections were used to reconstruct a full reference image.

- Projections measured between side and corner views are much more sensitive to a missing rod. This effect is in connection with the path length of the measured radiation in the fuel. The path length is largest for sides and corners and shorter between them. The shorter the path length the more sensitive is the projection to a missing rod.

5.5 Limited view problem

Because the number of views used for image reconstruction is smaller than ideally needed, the image density on the location of a missing rod is never zero. This yields an artifact produced by the algorithm. The larger the number of views, the smaller the artifact. The artifact is one of the main limiting factors of using section imaging technique for detection of a missing rod in a regular rod pattern. In the previous feasibility study /1/ criteria were determined for the number of views necessary for tomographic verification of 8 x 8 type BWR assemblies by detecting photons of different energies.

5.6 Evaluation techniques

Depending on the amount of measured data as well as on the accuracy of the measurement and on the type of the fuel assembly measured, there are different methods for evaluation of the images.

5.6.1 Visual evaluation

Visual evaluation of the image could provide a definite information about missing inner rods when the fuel assembly is homogeneous, the rod-to-rod burnup and the ^{154}Eu activity distribution are uniform, the sampling is fine (2 mm) and sufficient number of views (about 48) have been measured. This was the case in all of the measurements made under this task. Reconstructing images with different resolutions makes this visual evaluation even more reliable.

Fine scanning with steps of 2 mm makes it possible to reconstruct a high resolution image. This is necessary when details are needed. Due to the noise and the statistical fluctuations that appear in such an image, a smoothed image is preferred. The reconstruction algorithm provides an option to produce images of any resolution but not better than the one corresponding to the sampling parameter.

5.6.2 Intensity histograms

A composite histogram of the intensity deviation of each section image provides clear numerical information. A histogram shows the density distribution of all the pixels of the image. Local extreme values (min and max) are also calculated and displayed as bar charts (see Figure 8). Maximum values are shown in the upper right corner and minimum values in

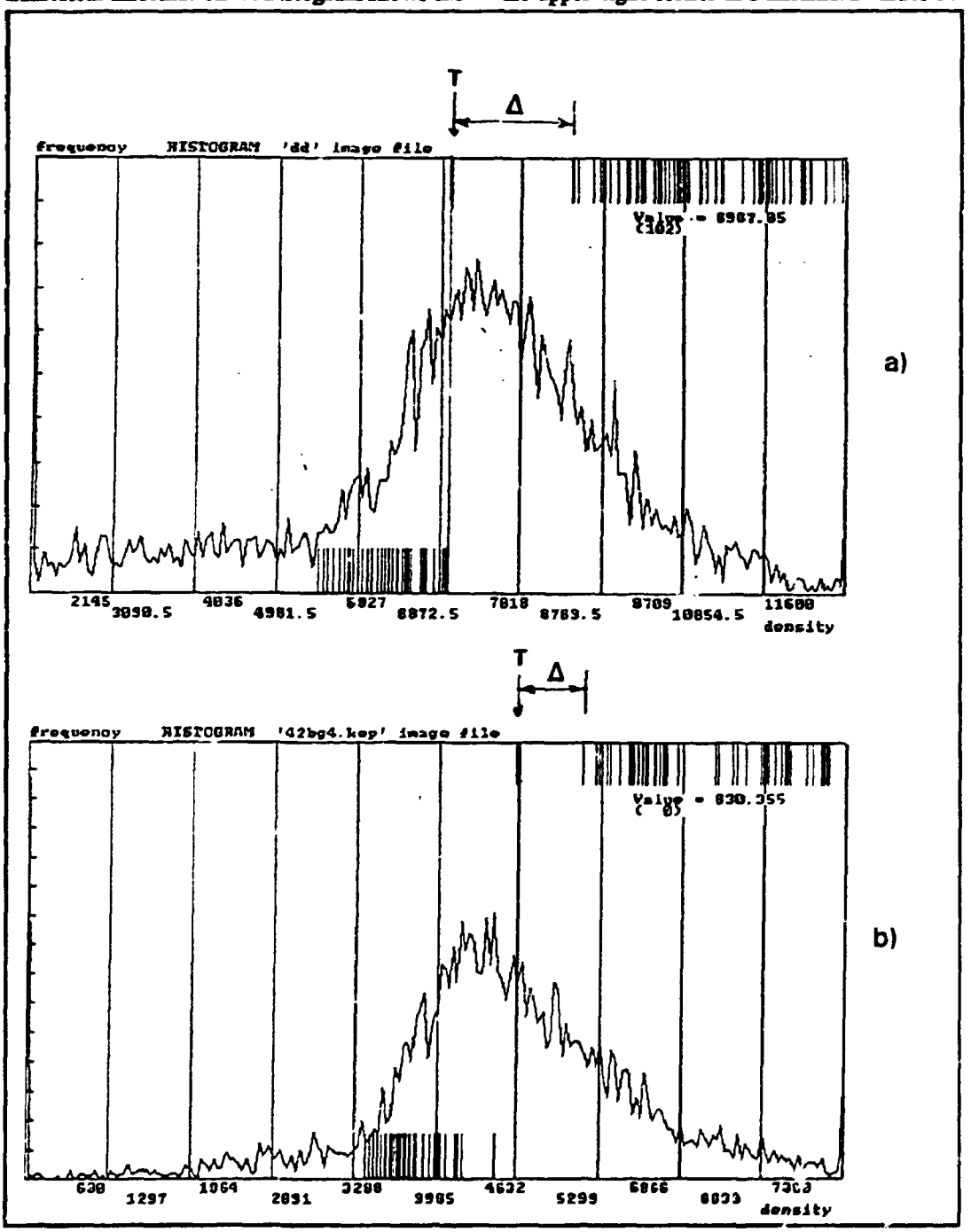

Figure 8. Density histograms for two sets of experimental data. In a) the number of views is 48 over 360°, in b) the number of views is 42 over 360°. Larger amount of views in a) results in a larger Δ and easier detection of a missing rod. T indicates the threshold level for binary image.

the lower left corner, respectively. Local maximum indicates an active point in the image, normally a fuel rod. Local minimum indicates an empty or low activity position, normally a position between the active rods.

When the image is of excellent quality, the largest minimal value is the density at the location of a missing rod. The values of the fuel rods (maximum values) are close to each other and separated from the value of the missing rod position. In most of the cases, however, there is a peak, an artifact, at the location of a missing rod. An artifact can be detected if it is definitely separated from the other maximum values which are close to each other in density. This separation is the Δ value in Figure 8. A large Δ provides a clear detection of a missing rod. A small Δ may lead to false detection.

In all of the cases, when a binary (black and white) section image is displayed, the threshold value T is set to the value of the minimum peak (see Figure 8). In a color display the whole density range can be clearly displayed for easier interpretation (see Figure 15 c), page 31). In case of a very non-uniform (rod-to-rod) activity distribution of the fuel assembly, the value of the separation may not be large enough. The only solution to increase the Δ-value is to increase the number of measured views.

6 SPENT FUEL MEASUREMENTS

Four measurement campaigns at the TVO KPA-STORE have been carried out using an underwater detector head /4 - 7/. During three of the campaigns, four different assemblies have been measured (Table I). References /2 - 3/ summarize the main results of these studies.

6.1 Fuel data

The BWR type assemblies measured are made by the ABB-Atom, Sweden and they have been irradiated by the TVO Power Company, Finland. This type of fuel has 63 fuel rods with external diameter of 11,75 mm or 12,25 mm and one special water filled inner rod (water rod) arranged in a square pattern of 8 x 8. The pellet external diameter is 10 or 10,5 mm. The external dimensions of the fuel channel are 139 mm x 139 mm. The declared parameters of the assemblies measured are given in Table I.

6.2 Hardware arrangement

The TVO KPA-STORE is a wet AFR storage for spent BWR fuel assemblies. It is equipped with an operator owned lift equipment, called gamma wagon, that is used for fuel service purposes. The gamma wagon is attached on a fixed position on the wall of the fuel receiving pond. Different fuel service fixtures can be clamped to the gamma wagon allowing the operator to move the assembly in vertical direction and also to rotate it manually. The measurement fixture used for tomographic studies holds the assembly during measurement.

The tomographic detector head was attached on a fixed position in the middle of the measurement fixture before lifting the equipment into the pond. Figure 9 shows the fixture being lowered into the pond. The fuel handling machine is used to transfer the assembly into the fixture. The precision of the axial rotation is $\pm$ 2°. Figure 10 shows the fuel assembly in the measurement position under water. The measurement geometry of the tomographic studies is shown in Figure 11 (page 23).

Table I. Declared parameters of the assemblies measured.

No.	Assembly ID	Measurement date	BU (MWd/kgU)	CT (years)	Fuel channel
1	9016	November 1990	33,2	3,5	no
2	8368	June 1991	31,6	2,1	yes
3	6130	June 1991	24,9	8,1	yes
4	7055	January 1993	17,7	9,5	yes

Figure 9. The stainless steel made tomographic measurement head is attached to the measurement fixture. The fixture is lowered by crane to the gamma wagon.

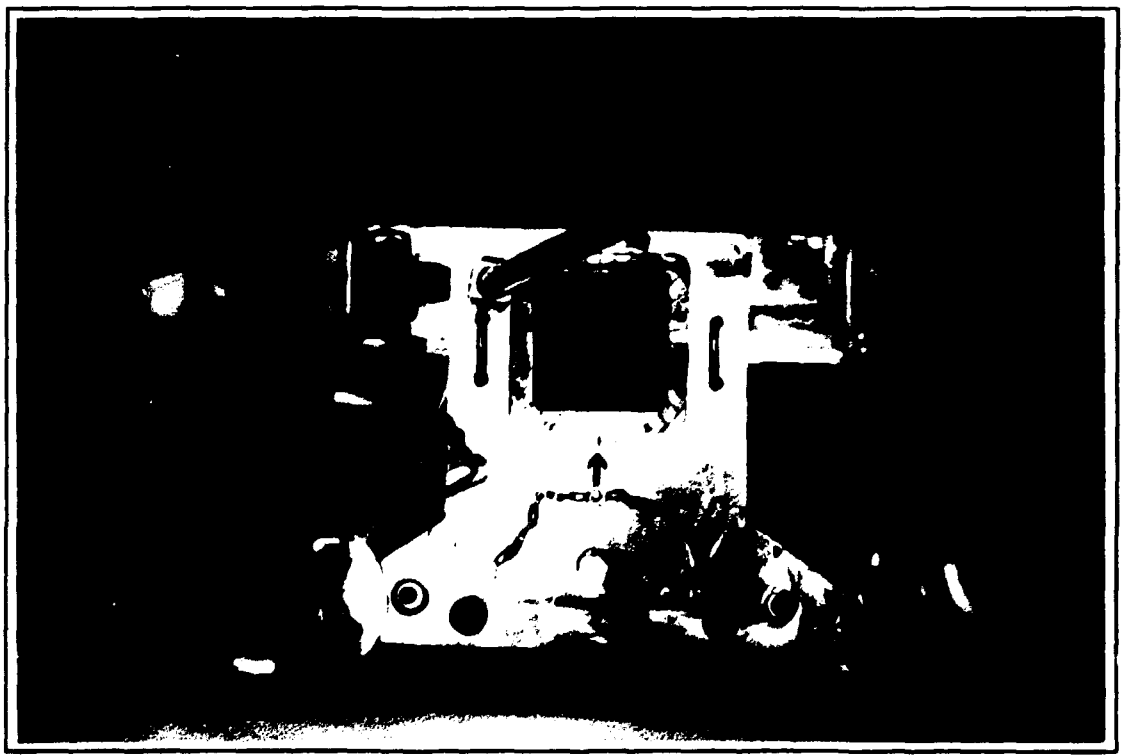

Figure 10. Measurement hardware at the TVO KPA-STORE seen from above. The assembly inside the fixture can be rotated manually by a steel bar seen on the top of the picture. The measurement head has a fixed position down in front of the assembly.

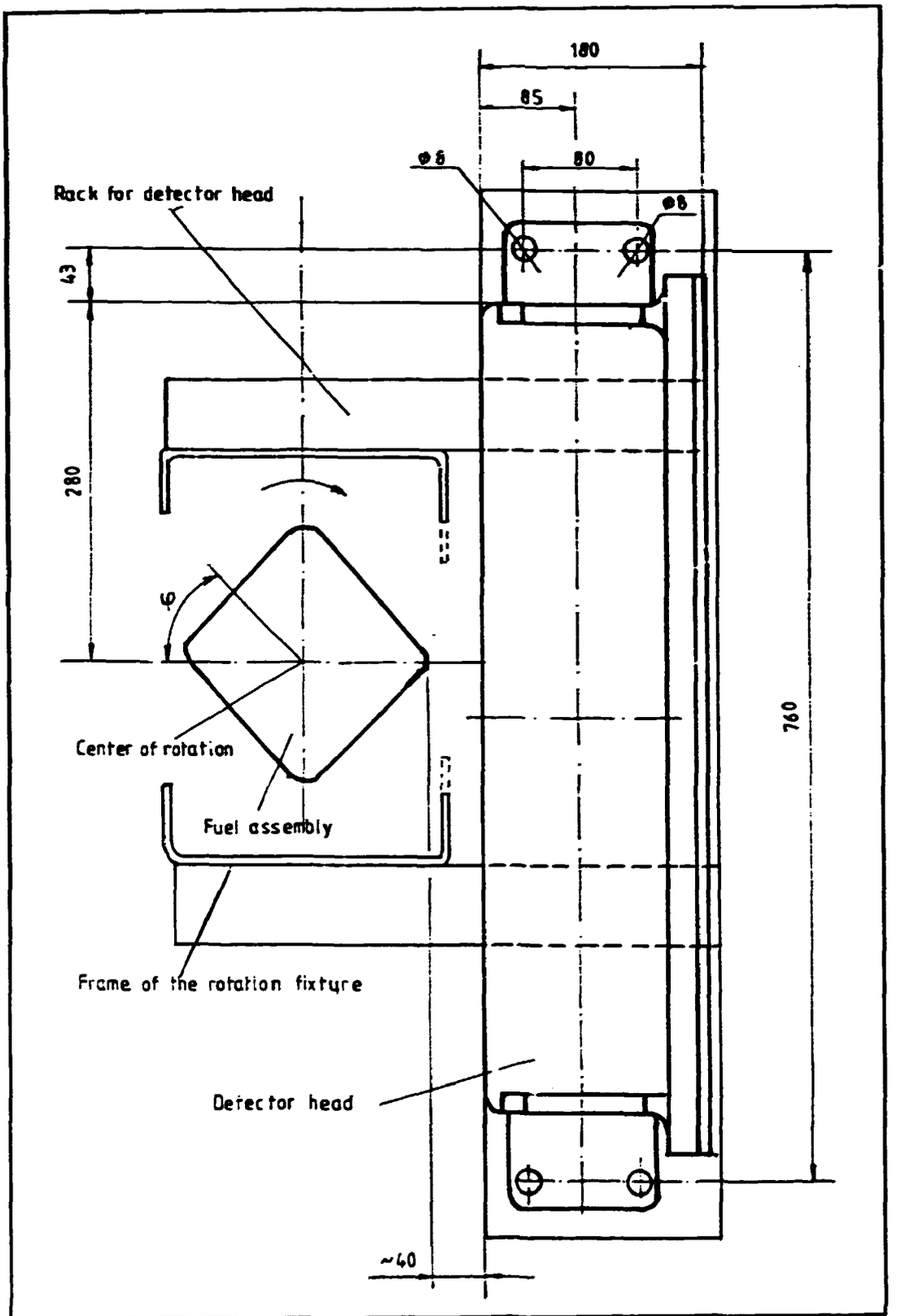

Figure 11. Geometry of the tomographic measurements at the TVO KPA-STORE.

6.3 Scanning results

6.3.1 Assembly no. 1

The measurements were performed during November 13 - 15, 1990. A single Si(Li) detector system with only one discriminator level was used for detection of the ^{144}Pr gamma rays of the short cooled fuel assembly 9016 (see Table I, page 21).

The following scanning parameters were used: Scanned total length at each view = 258 mm, steps between successive measurements = 2 mm, measurement time per point = 2 s. Scanning results are identified under filename "32 view" in Table II.

6.3.2 Assembly nos 2 and 3

The measurements were performed during June 18 - 19, 1991. A system of two Si(Li) detectors (a "small" one and a "large" one), each with three separate discriminator levels was used for measuring of the assemblies 8368 (no. 2) and 6130 (no. 3). The two detectors with different efficiencies allowed measurement of different activity levels without saturation. Discriminator levels were set for detection of Compton spectra of the following gamma activities. Above the lowest level a part of ^{137}Cs and ^{134}Cs photons are detected together with photons of ^{154}Eu and ^{144}Pr. Above the medium level photons of ^{154}Eu and ^{144}Pr are detected. Above the highest level photons only from ^{144}Pr are detected.

The two Si(Li) detectors were fixed along the same line, the smaller in front of the bigger one. Due to the geometry, both detectors detected the same position of the assembly through a common collimator slit. No data above the noise level were detected with the small detector for the assembly no. 3 with a long cooling time. Similarly, no ^{144}Pr photons were detected by either of the detectors from this assembly. The geometrical resolution of the detected signal is increasing with cooling time. A smearing effect related to short cooling times can be explained by the high level of unwanted scattering in the water.

The scanning parameters were as follows: The scanned total length at each view = 216 mm, steps between successive measurements = 2 mm, measurement time per point = 2 s. Scanning results are identified by filenames "bwr1-6" and "2bwr1-6" in Table II.

6.3.3 Assembly no. 4

The measurements were performed during January 19 - 20, 1993. An array of 10 CdTe detectors was used. Two discriminator levels were connected to each channel. The lower level allowed measuring both ^{154}Eu and ^{144}Pr gamma rays while the higher level allowed measuring only ^{144}Pr gamma rays.

The scanning parameters were as follows: The scanned total length at each view = 318 mm, steps between successive measurements = 20 mm, measurement time per point = 2 s. Scanning results are identified by filenames "PRA1.xxx" in Table II.

Typical activity profiles measured with a small Si(Li) detector for three sides of an assembly with 3,5 years cooling time are shown in Figure 12. Similar measured raw data for 8 detectors of the array of 10 CdTe detectors are shown in Figure 26 for an assembly with 9,5 years cooling time. Combining the discrete measurements of Figure 26 yields in activity profiles shown in Figure 27 for three different views.

6.4 Section images

Section images reconstructed from all the measured views can be seen in the upper part of Figures 13 - 25 and Figures 28 - 29. The lower parts of these figures show image density distribution along a line crossing the position of the missing fuel rod. The high DC signal levels seen in Figures 12 and 27 do not disturb the results. The difference between a black-and-white picture and a color picture can be

Table II. Main data of measured files.

No.	Assembly ID	Detector	Discriminator level (keV)	Measured scanning data file name	Image file name	No. of meas. views	Fig. no.
1	9016	small Si(Li)	700	32 view	32 view.1	32	13
2	8368	large Si(Li)	396	BWR1	II	48	14
3	"	"	621	BWR2	JJ LL	"	15 16
4	"	"	972,8	BWR3	KK	"	17
5	"	small Si(Li)	248	BWR4	NN	48	18
6	"	"	621	BWR5	MM PP	"	19 20
7	"	"	972	BWR6	OO	"	21
8	6130	large Si(Li)	250,6	2BWR1	BB DD DD (col)	48	22 23 15c
9	"	"	621	2BWR2	FF GG	"	24 25
10	"	"	972	2BWR3	-	"	-
11	"	small Si(Li)	248	2BWR4	-	48	-
12	"	"	621	2BWR5	-	"	-
13	"	"	972	2BWR6	-	"	-
14	7055	10 CdTe - det. no. 1 ... - det. no. 10 - full scan - full scan	250	 PRA1.D11 ... PRA1.D20 PRA1.S12 PRA1.S14	 PRA1G4.I ma PRA1G6.I ma	 48 "	26 27 28 29
15	"	10 CdTe - det no. 1 ... - det. no. 10	700	 PRA1.D01 ... PRA1.D10	 - ... -	 48 "	-

seen by comparing Figures 23 and 15c which show the same image "dd".

All the section images reconstructed from data measured by the large Si(Li) detector are very similar. Further evaluation showed that the sensitivity of this detector was decreased due to its small thickness for the high energy gamma rays. This phenomenon is related to the images based mostly on the ^{154}Eu gamma activity distribution. Figures 14 - 17 are all measured by the large Si(Li) detector. From the similar results of the three measurements with three different thresholds the effect can be seen.

The small Si(Li) detector has a thickness double of that of the large Si(Li) and it had a better spectral response. In the images reconstructed from these measurements (Figures 18 - 21) the different energy absorption due to the three measured ranges (threshold levels) can be detected.

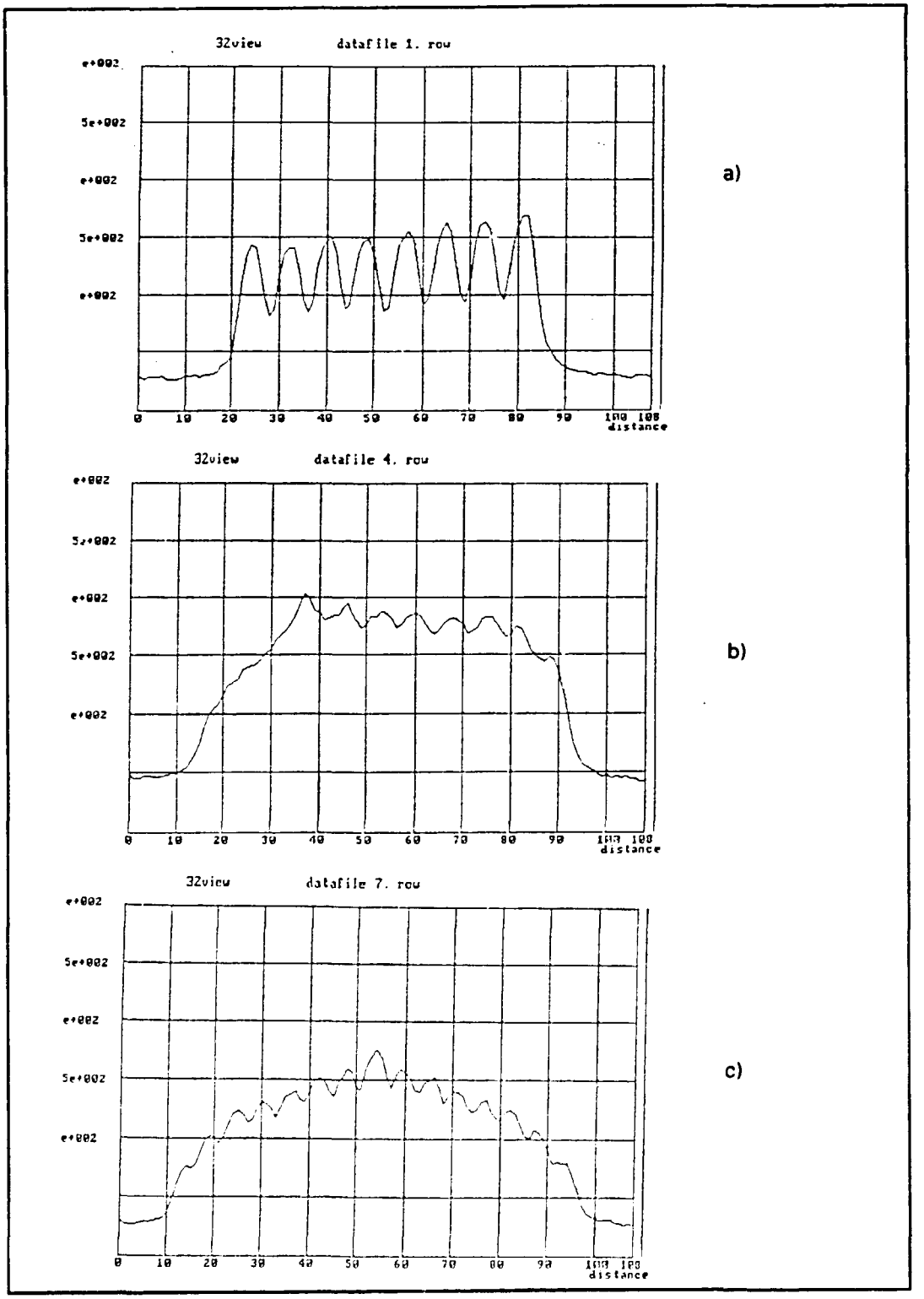

Figure 12. *Activity profiles measured with a small Si(Li) detector for three sides of a BWR assembly with 3,5 years cooling time.* ***a)*** $\varphi = 0°$ *(flat side),* ***b)*** $\varphi = 22{,}5°$ *and* ***c)*** $\varphi = 45°$ *(corner).*

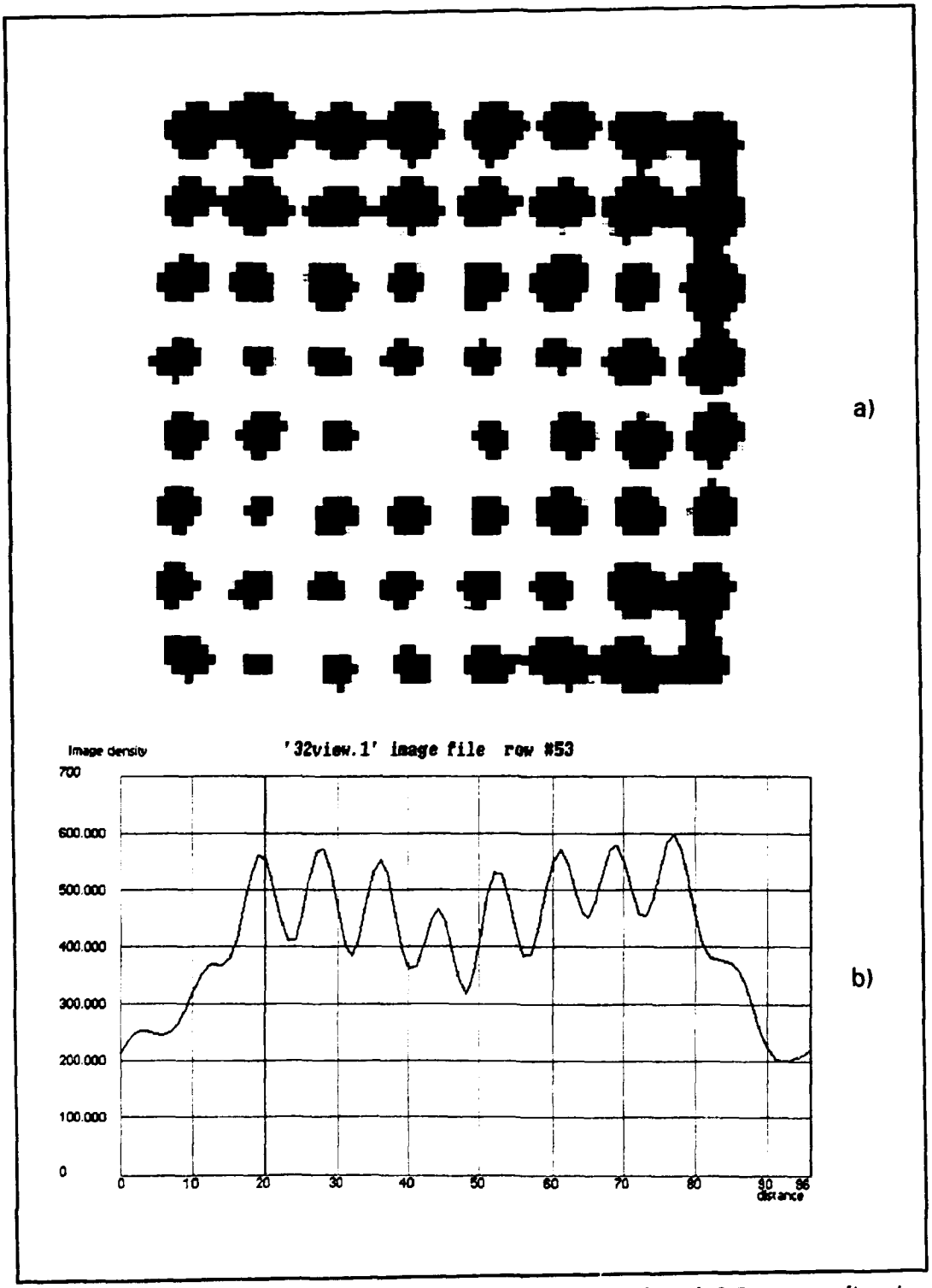

Figure 13. a) ^{144}Pr *activity cross section image of a BWR assembly with 3,5 years cooling time constructed from 32 views measured by a small Si(Li) detector.* ***b)*** *Activity profile across the rod row including the water filled rod. Threshold = 700 keV.*

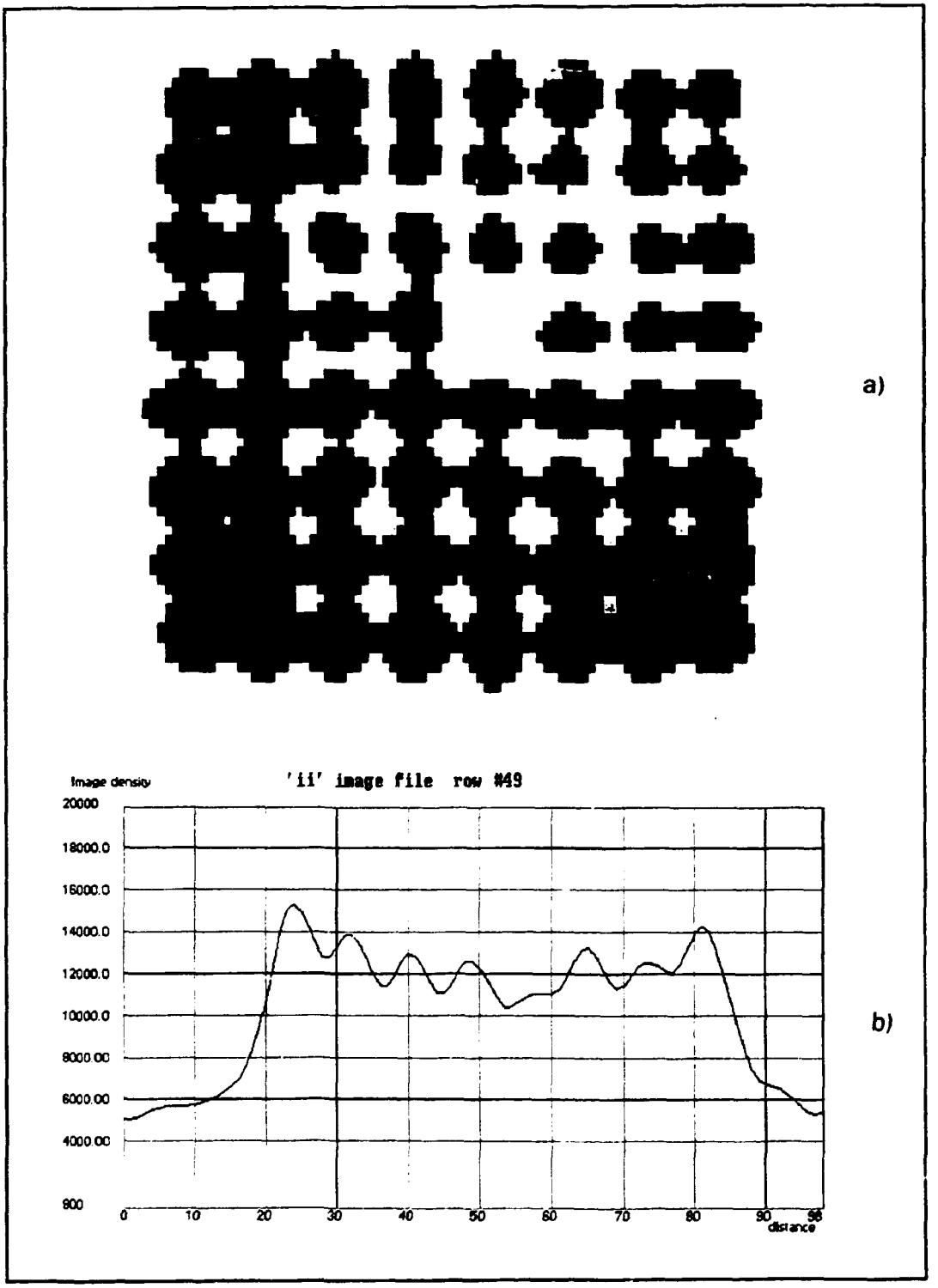

Figure 14. a) *^{154}Eu activity cross section image of a BWR assembly with 2,1 years cooling time constructed from 48 views measured by a large Si(Li) detector.* ***b)*** *Activity profile across the rod row including the water filled rod. Threshold = 396 keV.*

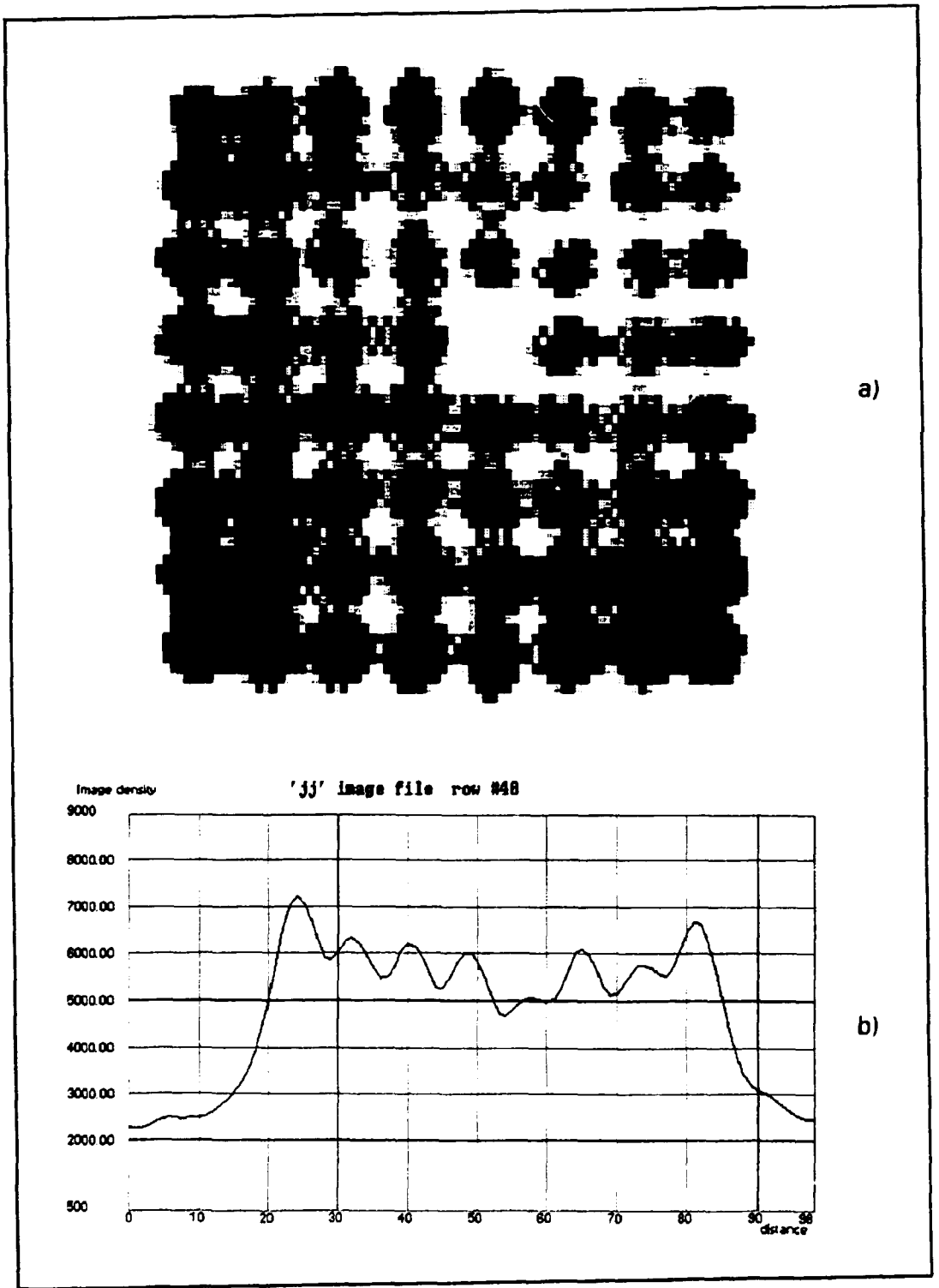

Figure 15. *a) Low resolution ^{154}Eu activity cross section image of a BWR assembly with 2,1 years cooling time constructed from 48 views measured by a large Si(Li) detector. b) Activity profile across the rod row including the water filled rod. Threshold = 621 keV.*

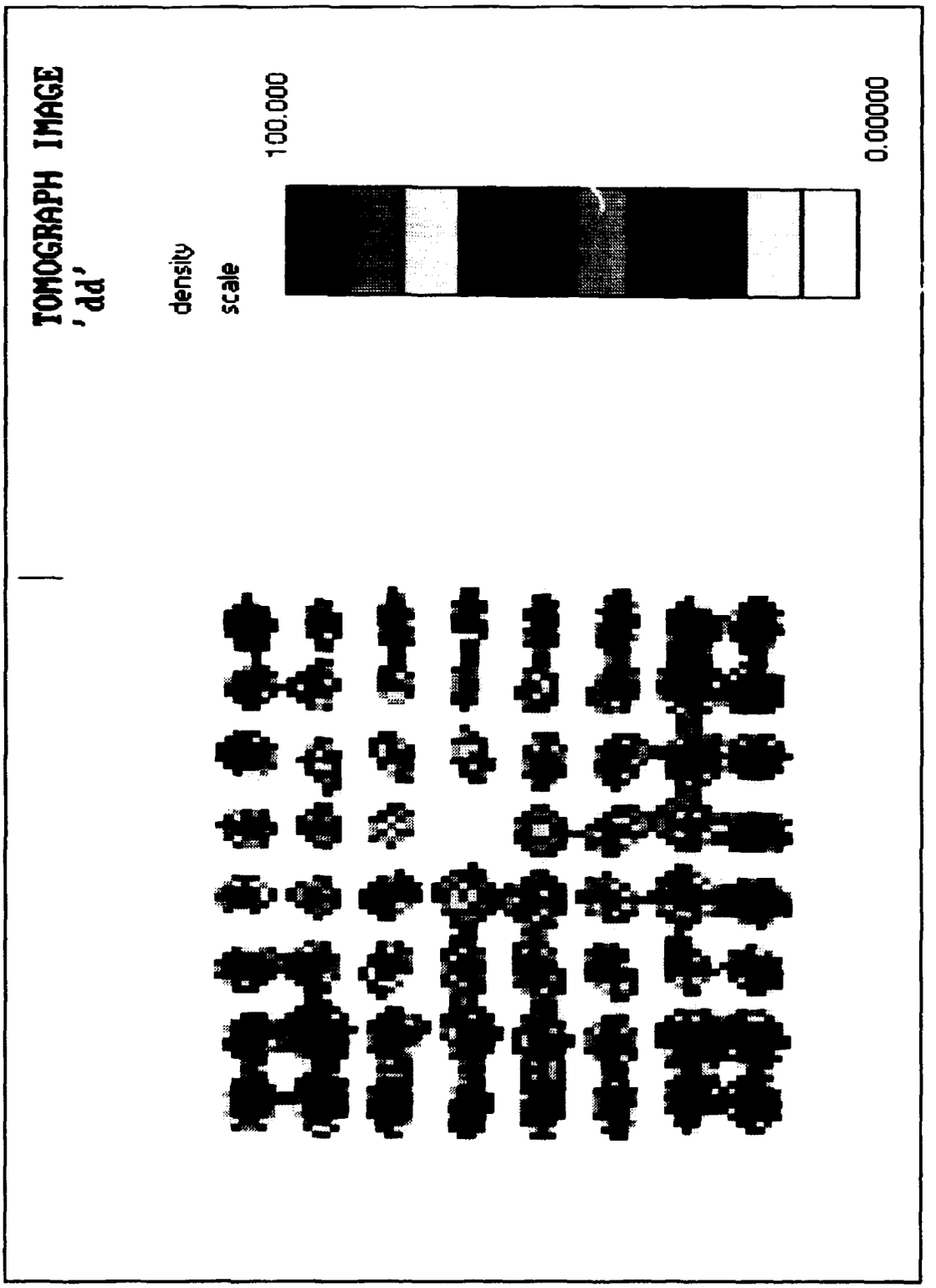

Figure 15 c). *Low resolution ^{154}Eu activity cross section color image of a BWR assembly with 8,1 years cooling time constructed from 48 views measured by a large Si(Li) detector. Threshold = 250,6 keV. A monochrome version of this image can be seen in Figure 23 a) (page 39).*

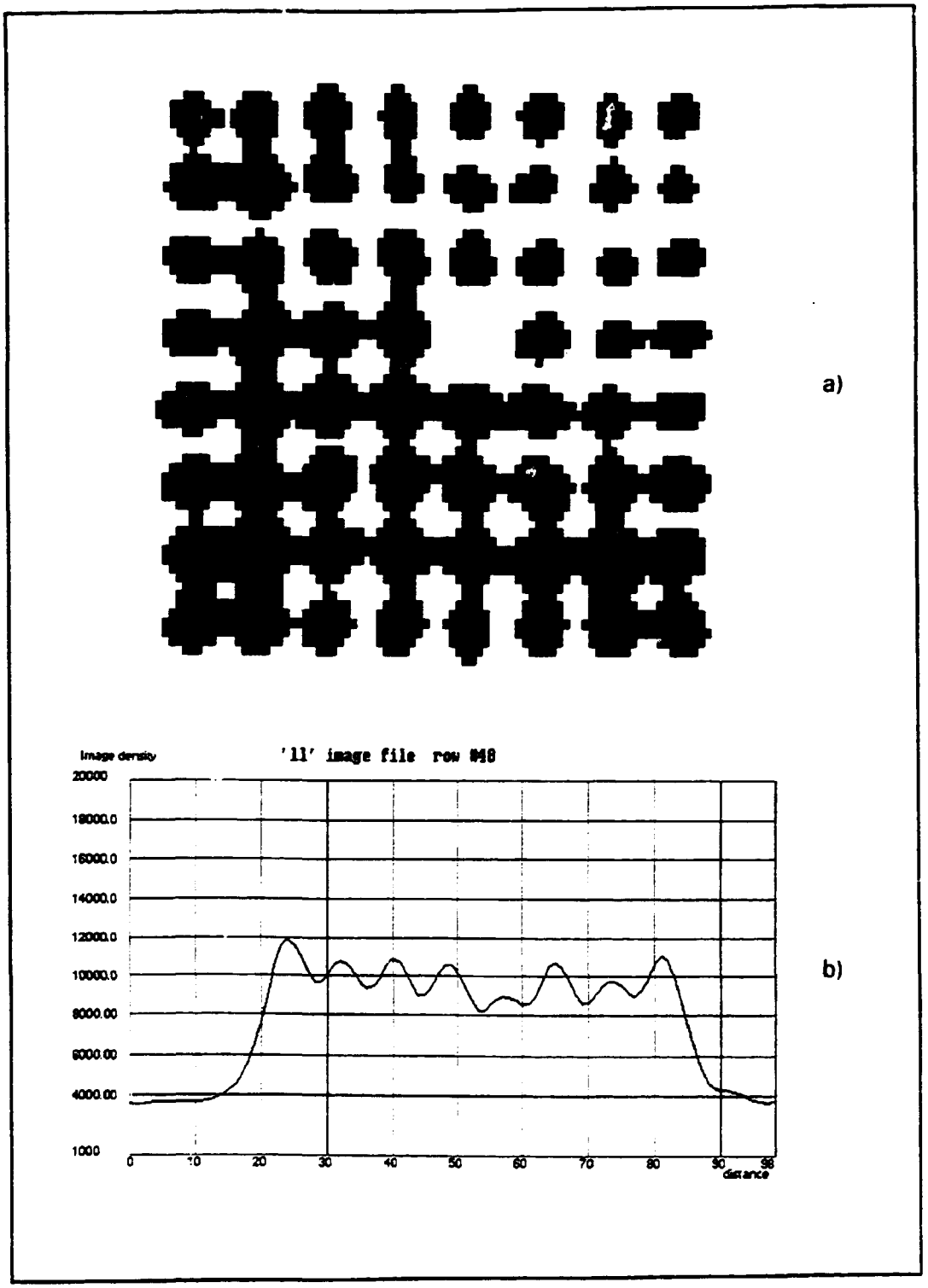

Figure 16. a) *^{154}Eu activity cross section image of a BWR assembly with 2,1 years cooling time constructed from 48 views measured by a large Si(Li) detector.* ***b)*** *Activity profile across the rod row including the water filled rod. Threshold = 621 keV.*

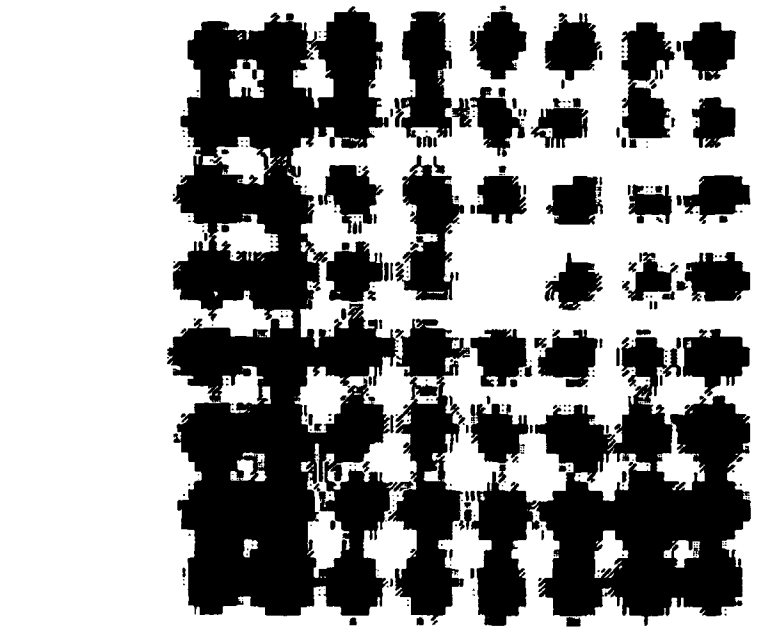

a)

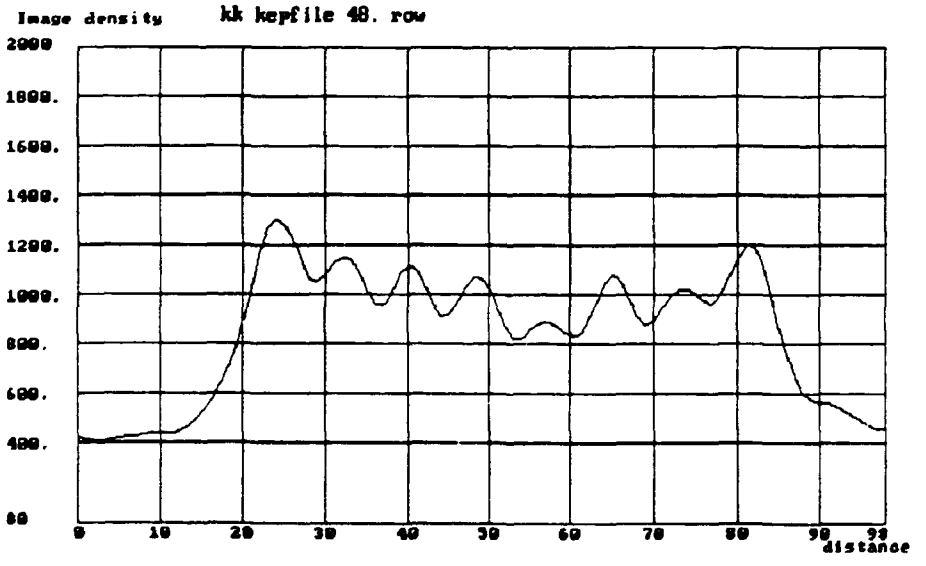

b)

Figure 17. a) *^{154}Eu activity cross section image of a BWR assembly with 2,1 years cooling time constructed from 48 views measured by a large Si(Li) detector.* ***b)*** *Activity profile across the rod row including the water filled rod. Threshold = 972,8 keV.*

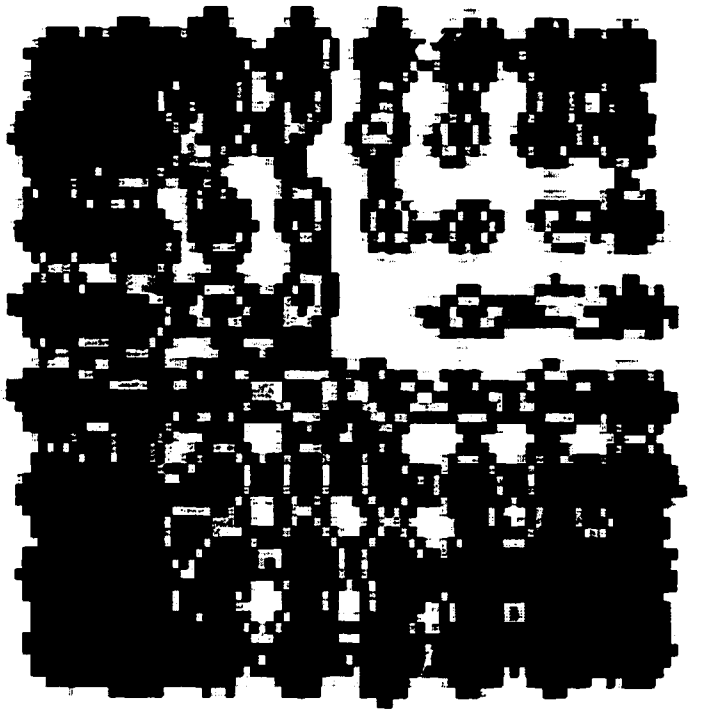

a)

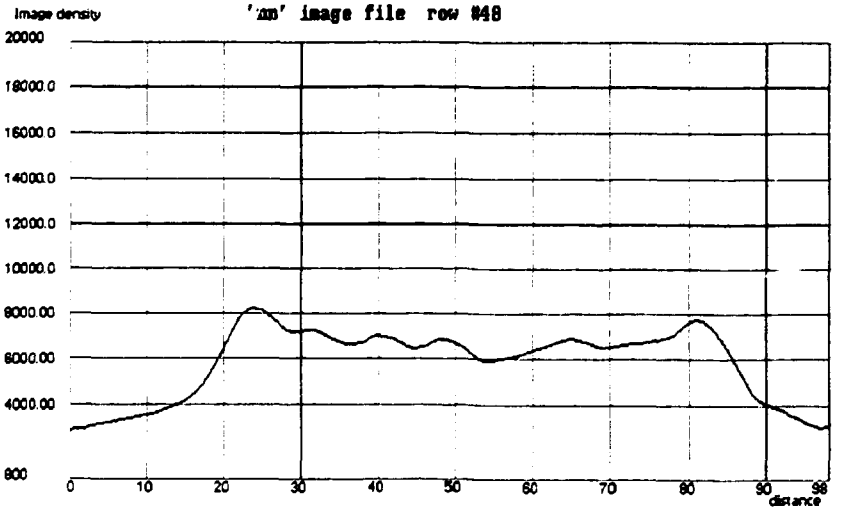

b)

Figure 18. a) *Low resolution ^{144}Pr activity cross section image of a BWR assembly with 2,1 years cooling time constructed from 48 views measured by a small Si(Li) detector.* ***b)*** *Activity profile with bad statistics across the rod row including the water filled rod. Threshold = 248 keV.*

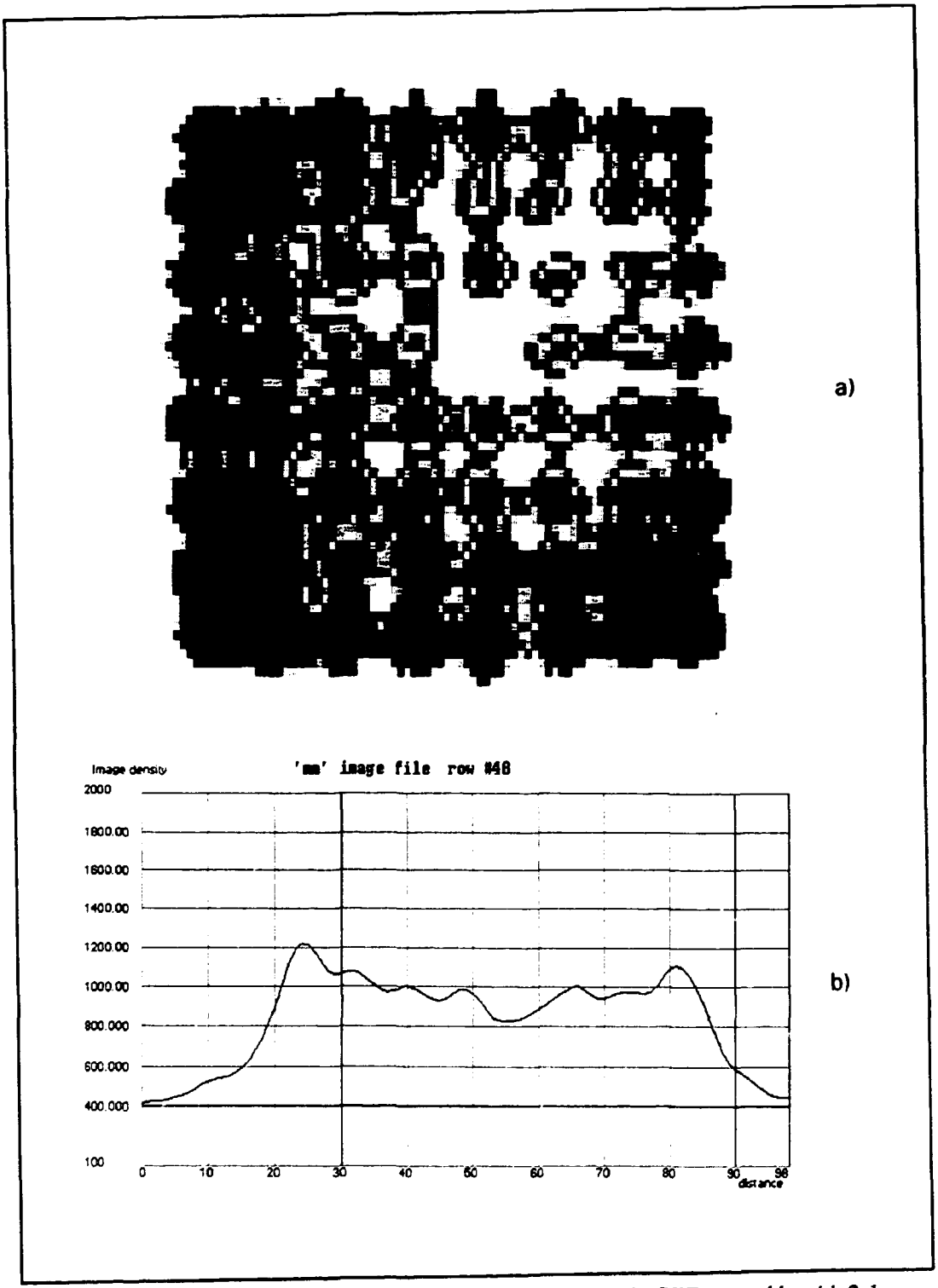

Figure 19. a) *Low resolution ^{144}Pr activity cross section image of a BWR assembly with 2,1 years cooling time constructed from 48 views measured by a small Si(Li) detector.* ***b)*** *Activity profile with bad statistics across the rod row including the water filled rod. Threshold = 621 keV.*

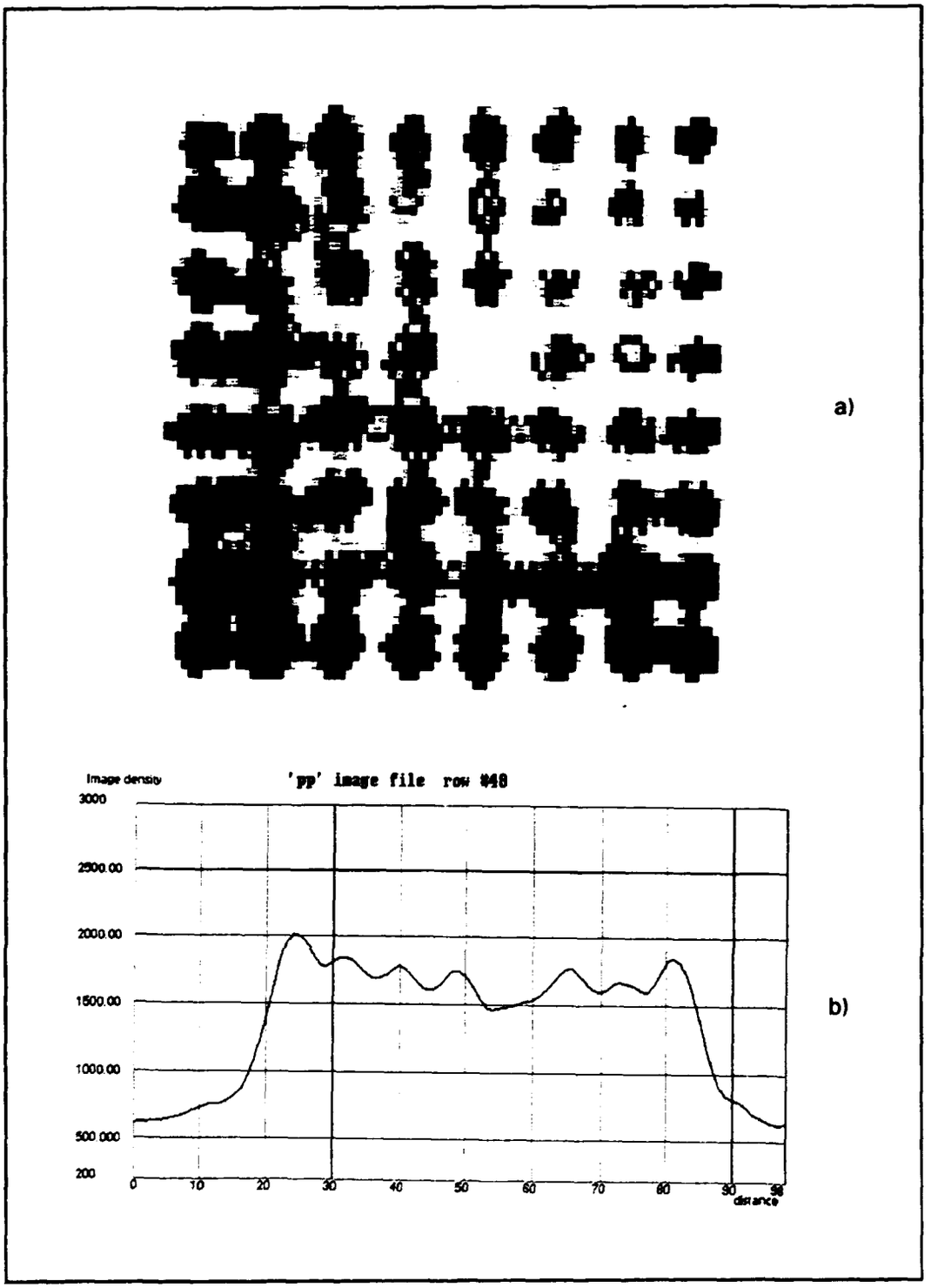

Figure 20. *a) Medium resolution ^{144}Pr activity cross section image of a BWR assembly with 2,1 years cooling time constructed from 48 views measured by a small Si(Li) detector.* ***b)*** *Activity profile with bad statistics across the rod row including the water filled rod. Threshold = 621 keV.*

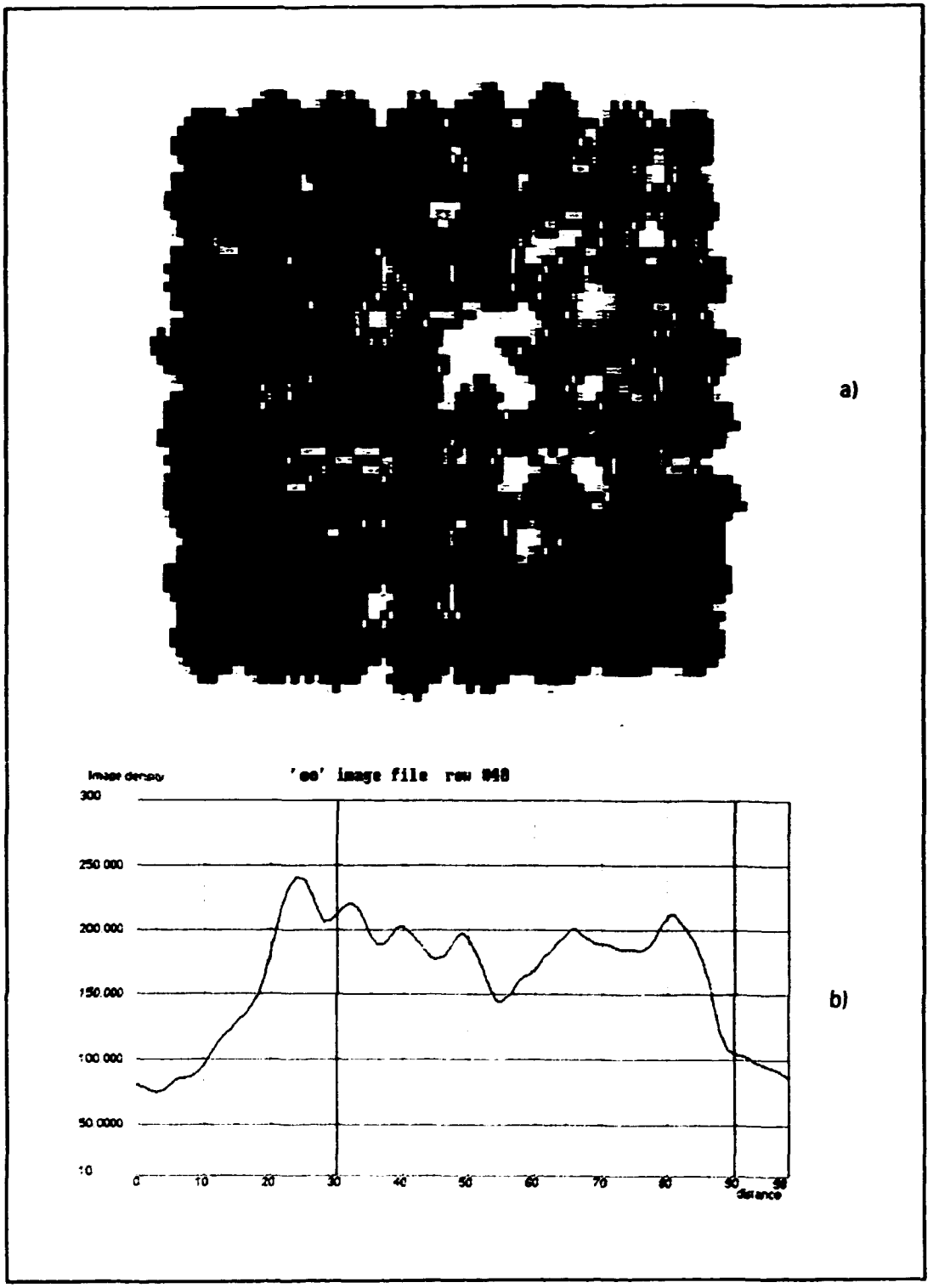

Figure 21. a) Low resolution ^{144}Pr activity cross section image of a BWR assembly with 2,1 years cooling time constructed from 48 views measured by a small Si(Li) detector. b) Activity profile with bad statistics across the rod row including the water filled rod. Threshold = 972 keV.

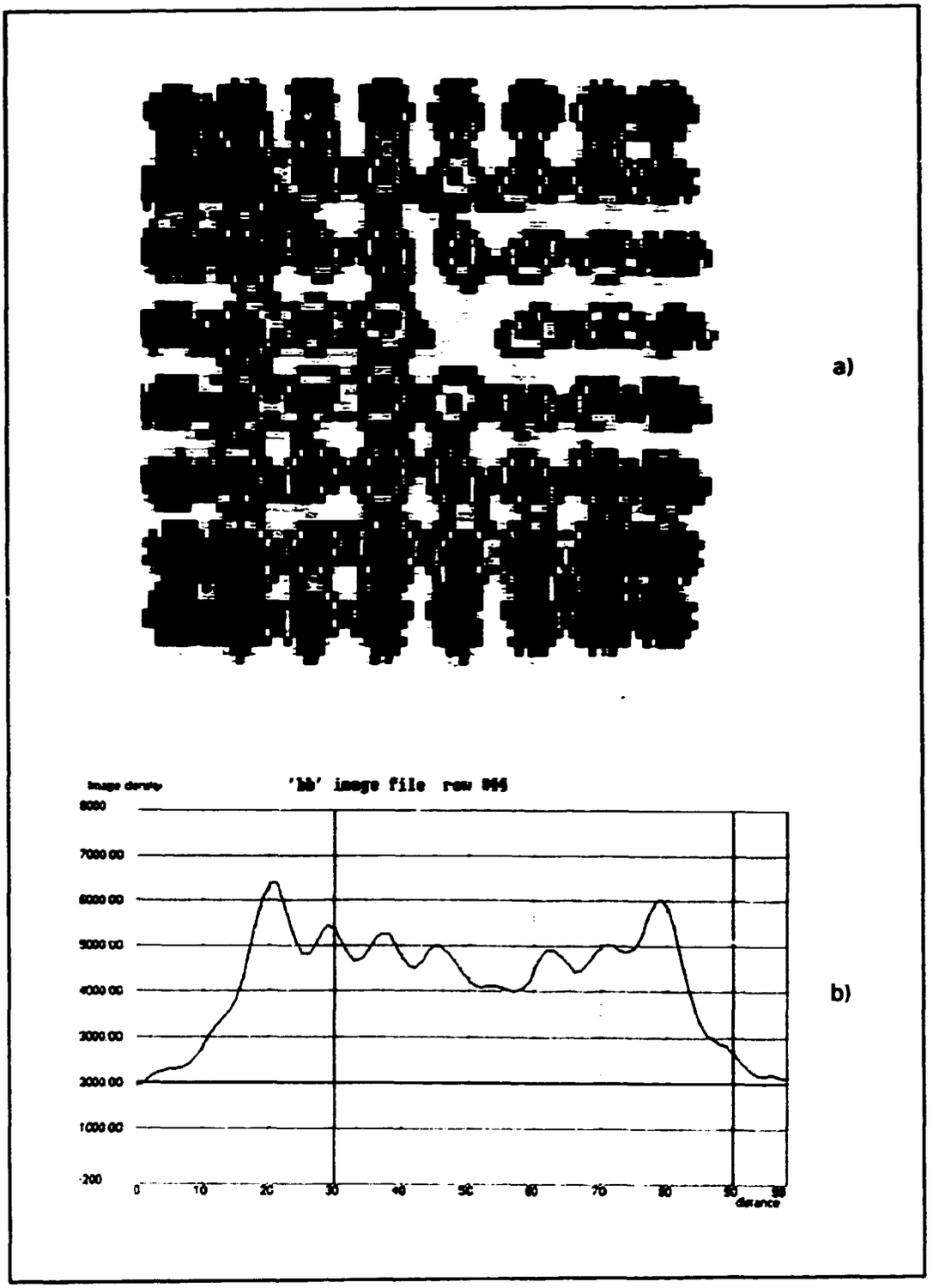

Figure 22. a) Medium resolution ^{154}Eu activity cross section image of a BWR assembly with 8.1 years cooling time constructed from 48 views measured by a large Si(Li) detector. b) Activity profile across the rod row including the water filled rod. Threshold = 250.6 keV.

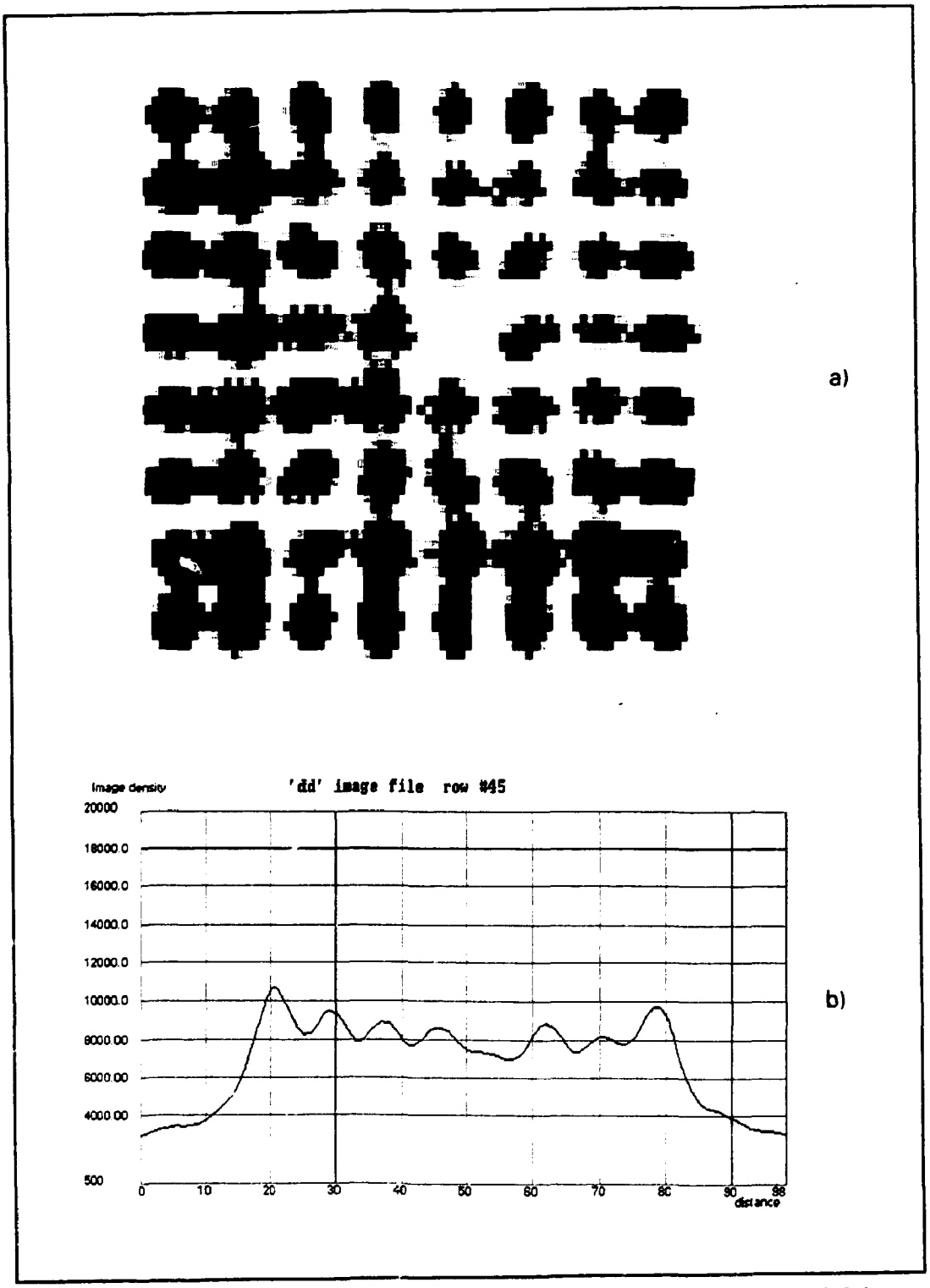

Figure 23. a) *Low resolution ^{154}Eu activity cross section image of a BWR assembly with 8,1 years cooling time constructed from 48 views measured by a large Si(Li) detector.* ***b)*** *Activity profile across the rod row including the water filled rod. Threshold = 250,6 keV. A colour version of image 23 a) can be seen in Figure 15 c) (page 31).*

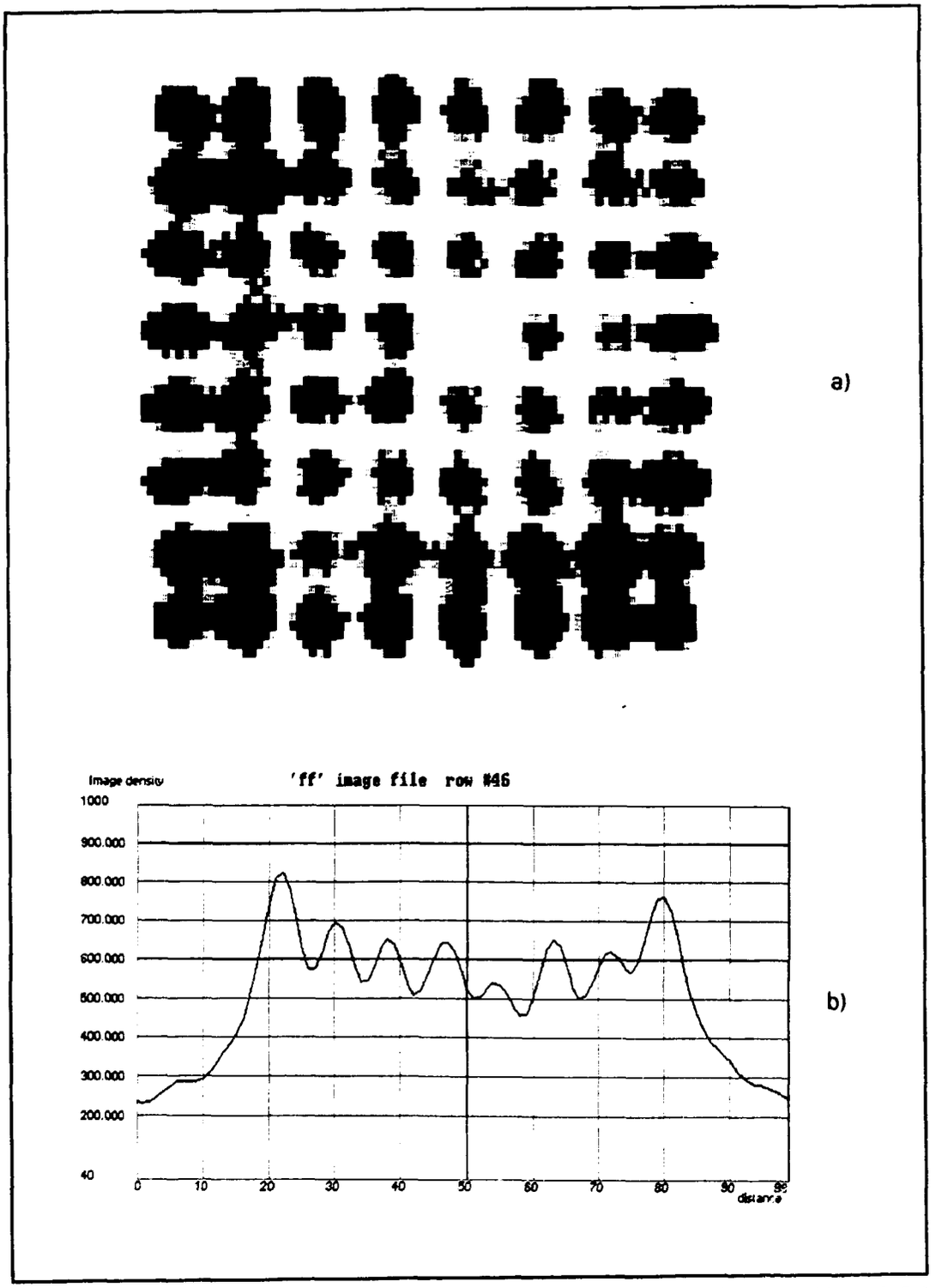

Figure 24. *a) Medium resolution ^{154}Eu activity cross section image of a BWR assembly with 8,1 years cooling time constructed from 48 views measured by a large Si(Li) detector.* ***b)*** *Activity profile across the rod row including the water filled rod. Threshold = 621 keV.*

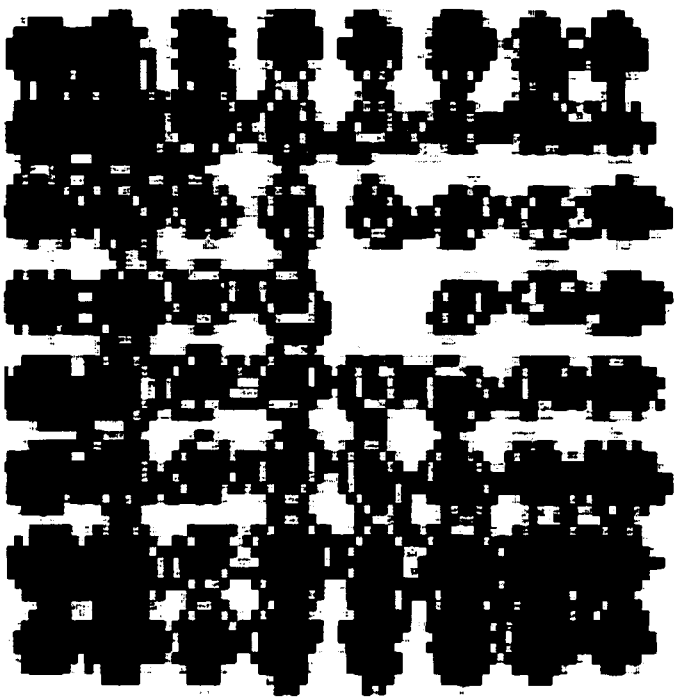

a)

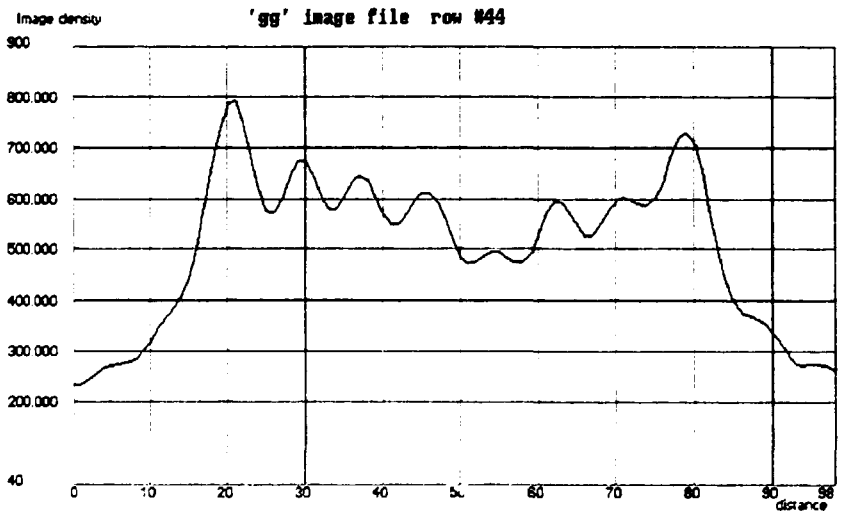

b)

Figure 25. a) *Low resolution ^{154}Eu activity cross section image of a BWR assembly with 8,1 years cooling time constructed from 48 views measured by a large Si(Li) detector.* ***b)*** *Activity profile across the rod row including the water filled rod. Threshold = 621 keV.*

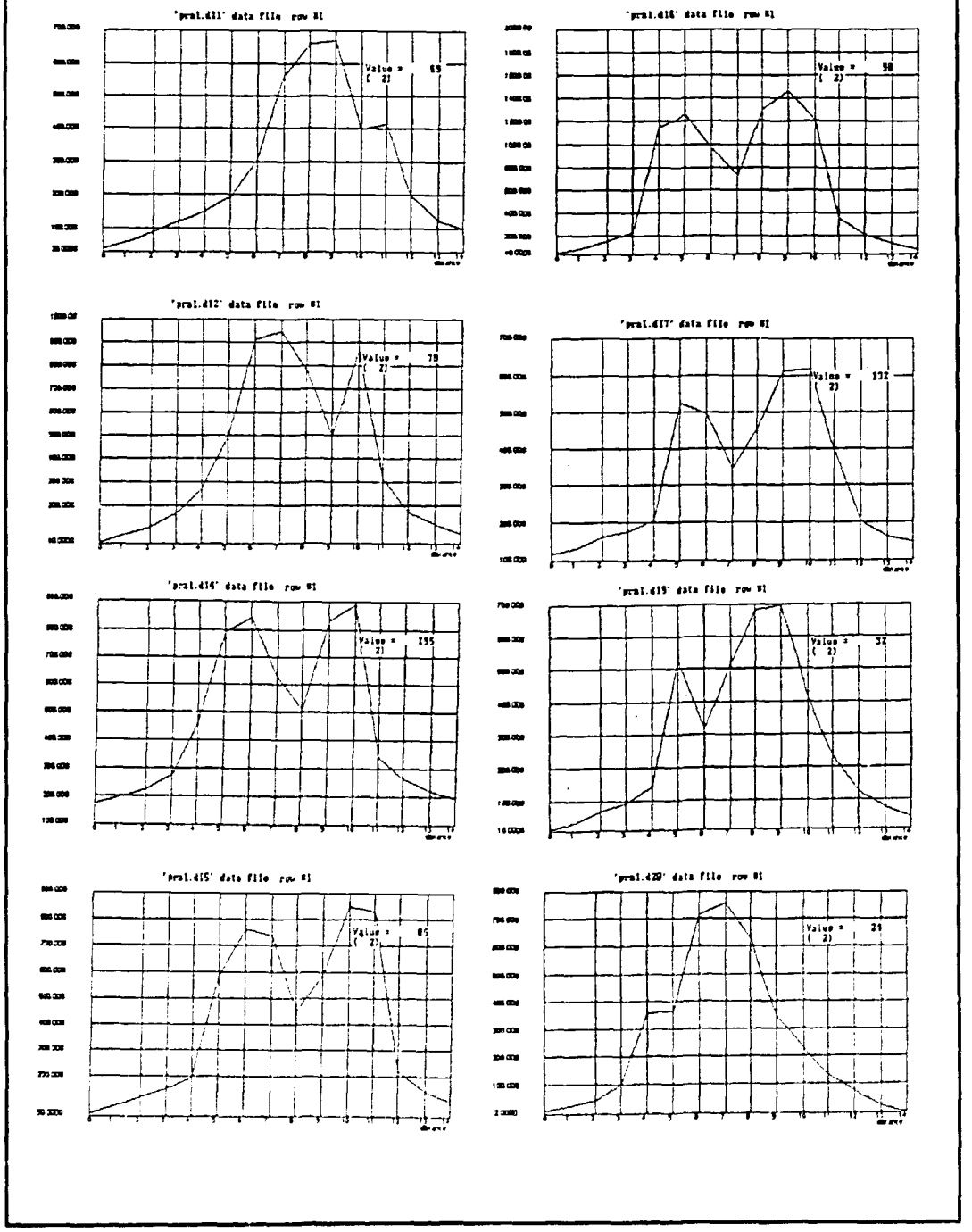

Figure 26. Discrete readings of eight CdTe detectors along a flat side of a BWR assembly with 9,5 years cooling time. Step between successive measurements was 20 mm.

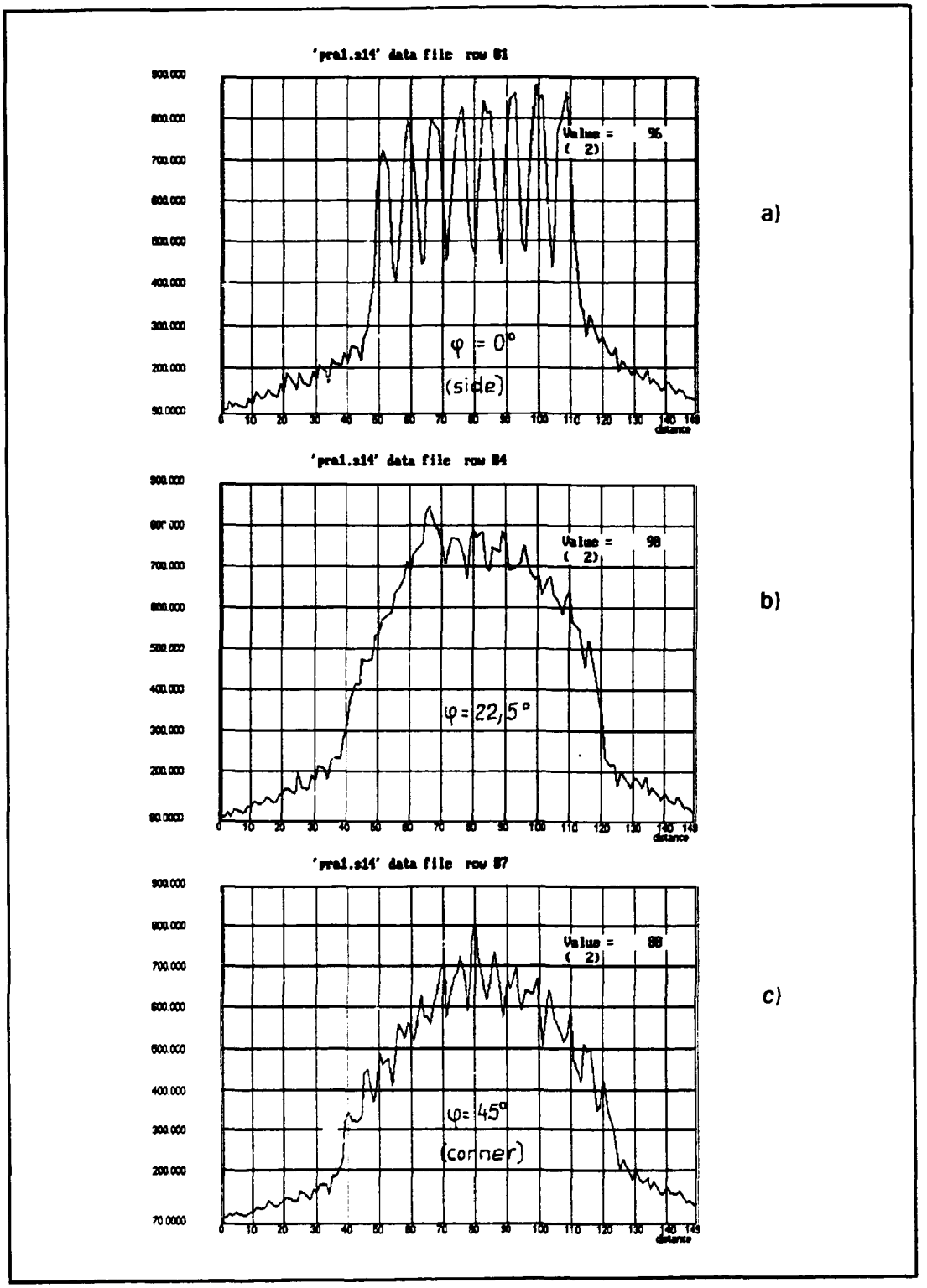

Figure 27. *Activity profiles combined from the measured readings of 10 CdTe detectors (see Figure 26) for three sides of a BWR assembly with 9,5 years cooling time.* ***a)*** $\varphi = 0°$ *(flat side),* ***b)*** $\varphi = 22{,}5°$ *and c)* $\varphi = 45°$ *(corner).*

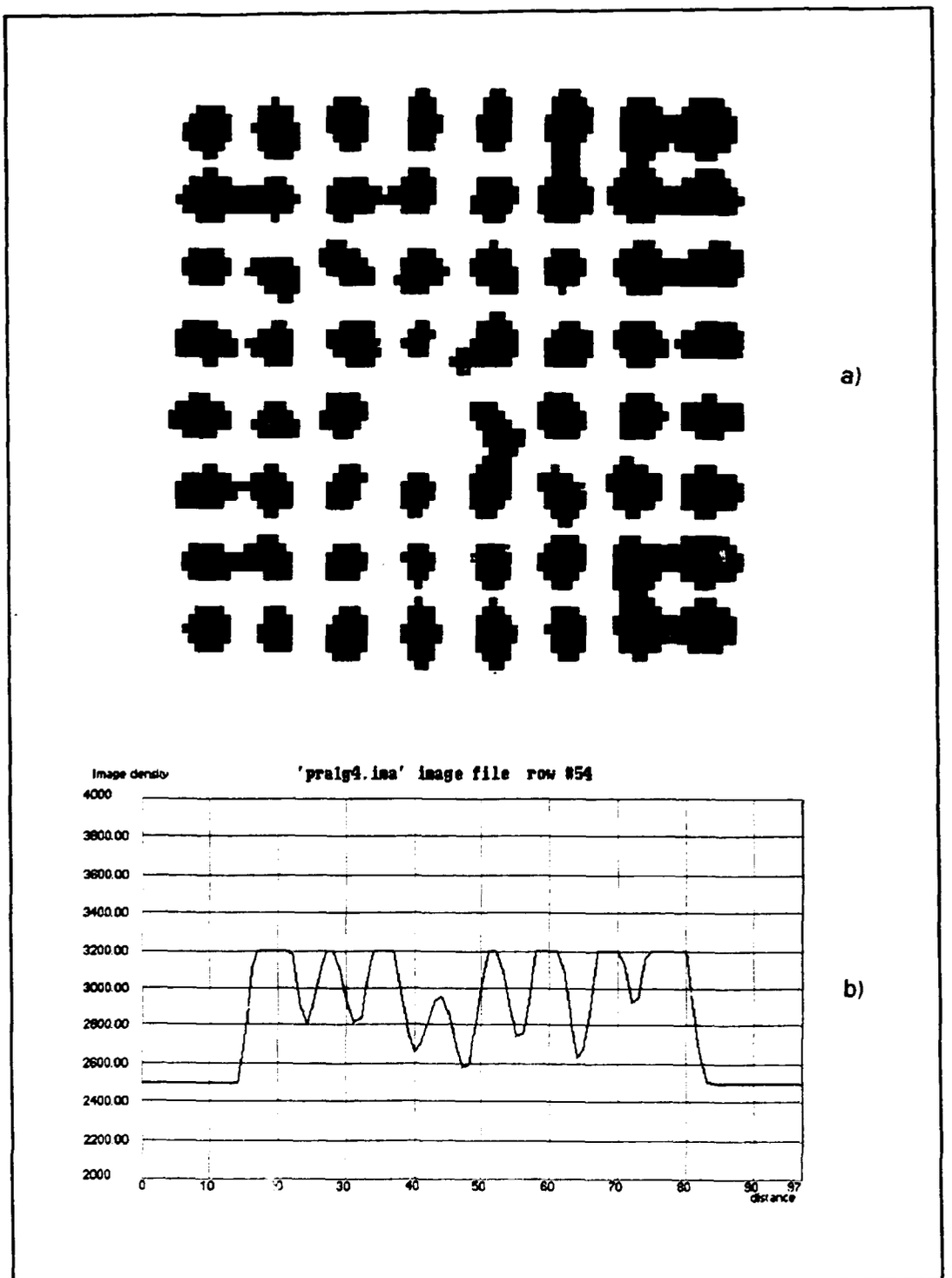

Figure 28. *a) Medium resolution ^{154}Eu activity cross section image of a BWR assembly with 9,5 years cooling time constructed from 48 views measured by an array of 10 CdTe detectors.*
b) Activity profile across the rod row including the water filled rod. Threshold = 250 keV. The flat tops of the activity profile (b) do not indicate saturation. They have been cut in the calculation process.

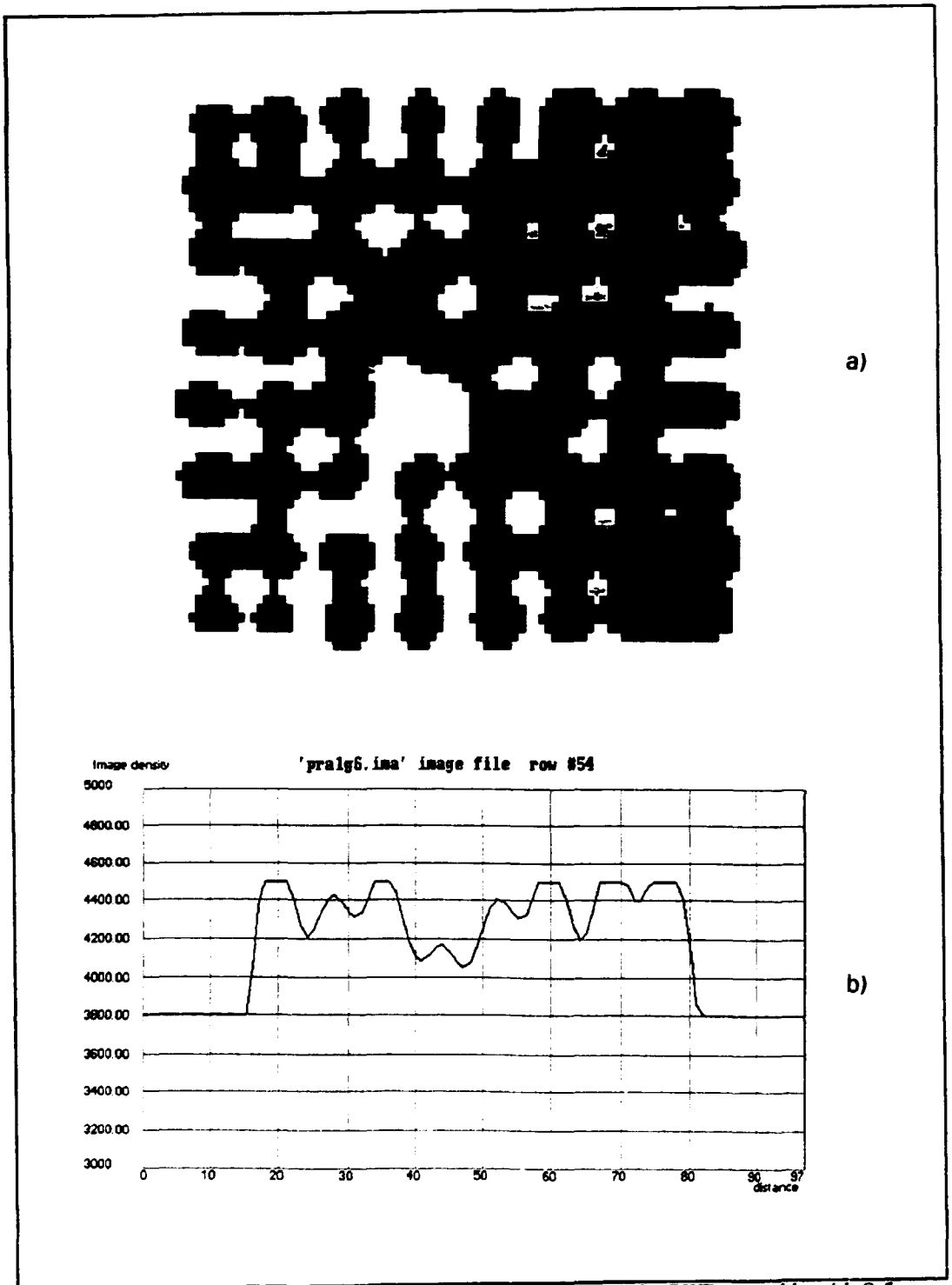

Figure 29. a) *Low resolution ^{154}Eu activity cross section image of a BWR assembly with 9,5 years cooling time constructed from 48 views measured by an array of 10 CdTe detectors.* ***b)*** *Activity profile across the rod row including the water filled rod. Threshold = 250 keV. The flat tops of the activity profile (b) do not indicate saturation. They have been cut in the calculation process.*

6.5 Evaluation of images

Measurements provided results for fuel assemblies of different cooling times. Section images reconstructed reflected the ^{154}Eu and ^{144}Pr distributions and in many cases a mixture of these components. The ^{137}Cs + ^{134}Cs contribution can be considered as not significant due to the shorter part of the compton spectra measured and the higher weight of the higher energy photons.

All the measured views were used to reconstruct the images. In some of the cases, mainly when ^{144}Pr is the main component, a smaller number of views would, however, be enough. Large number of views provides reliable detection of a missing rod and makes the measurement also less sensitive to some important parameters influencing the image quality. They include the geometrical and statistical accuracy and the fact that the detected photon can be any mixture of the Eu/Pr gamma rays, even with some Cs contribution included. Separation of all gamma rays is difficult.

For fuel with a short cooling time (2 and 3,5 years), ^{144}Pr can be detected and it provides a reliable detection with 32 measured views. When 48 views are measured, ^{154}Eu can also be used. The higher absorption of these gamma rays is compensated by the better statistical accuracy. In the case of 2 years cooling time, a high level of unwanted scattering in water is also detected and it is causing smearing of the detected activity profile. In the case of a long cooling time (8 years), mostly ^{154}Eu is detected. When 48 views are used, some ^{137}Cs + ^{134}Cs contribution is included because the threshold level was lowered to increase the count rate of the long cooled assembly. No ^{144}Pr gamma rays can be detected after such a long cooling time.

All measured scanning files which provided signal above the noise level could also be used to reveal the position of the missing inner rod. This is due to the fact that mostly high energy gamma rays (^{154}Eu and ^{144}Pr) are detected. The higher the energy, the higher the effect caused by a missing rod. This can be seen clearly in the ^{144}Pr image of Figure 21 where, in spite of the very bad statistics, the noisy image provides a clear indication of a missing rod.

7 PROCEDURE FOR PARTIAL DEFECT TEST

It has been shown that the method studied using passive gamma emission tomography for mapping non-destructively the rod structure of a spent BWR assembly can be used for safeguards purposes i.e. for partial defect verification. A partial defect, in general terms, is understood to mean missing of some (not all) of the fuel material. The IAEA definition for partial defect test of spent LWR fuel at the present time requires a capability to reveal missing of 50 % or more of the irradiated nuclear material.

7.1 Equipment

When tomography is considered for partial defect verification using the method studied, the following equipment and instrumentation is needed. An apparatus to measure gamma emission of spent fuel assemblies under water using an underwater detector head. This includes also hardware to hold and rotate the assembly during the measurement. Electronic instrumentation is needed together with a computer to control the measurement, store data and run the data analysis programs.

There are several ways to arrange the assembly holding and rotation depending on the local possibilities. Either the assembly is rotated around its own axis in front of the detector head or the detector system is rotated around the assembly. In all cases the assembly needs to be lifted or moved from the storage position either partly or completely.

7.2 Position of detector head

The underwater measurement head needs to be installed in a position where assemblies can be held and rotated during measurement. A facility specific arrangement, like the gamma wagon at the TVO facilities in Finland (see Figure 10, page 22) can be used for this purpose. Assemblies of short and long cooling times need to be scanned at 48 views over rotation of 360°. It is recommended that the present type of detector head has a fixed position in the pond allowing good geometrical positioning. The head can be installed under water using any facility specific solution if a gamma wagon type hardware is not available.

7.3 Rotation with fuel handling machine

Fuel assemblies can be held and rotated also by the fuel handling machine, while the detector head has a fixed position. There may be differences or limitations in the basic scanning approach using this option. The algorithms can, however, take such limitations into account during the data analysis.

At the TVO KPA-STORE the fuel handling machine can rotate the assembly only in the range 0° - 310°. The steps of rotation can be any, but in practice only steps of either 5° or 10° are easy to be set in a repeatable way. Radial precision of angle setting is ± 2°.

Computer simulation was made to study the feasibility of using the fuel handling machine for rotation at TVO. The results show that the reduced range of the scanning angles means smaller sensitivity. This can partially be compensated by increasing the number of views within the scanned range. In the range 0° - 310° this can be compensated fully. About 60 views over 310° provides as good sensitivity as 48 views over the range of 360°. Simulation results demonstrated also, that if the number of total views exceeds about 40 (and this was always the case in practical measurements), the accuracy of 5° ± 2° is acceptable for image reconstruction.

Concerning the limited range of angles, the image reconstruction program can accept irregular angular sampling. As an example, alternating steps of 5° and 10° of rotational angles can provide similar results as the even spaced steps of 7,5°.

7.4 On-site image calculation

Measurement data are stored by the computer used. Based on this information, the image reconstruction and evaluation can be done automatically and it takes only a few minutes after completing of scanning. The cross sectional image can thus be constructed while the assembly is still in the measurement position.

8 LIMITATIONS AND POSSIBILITIES

The measurement system used was designed for experimental purposes. Even the present system can be used, if needed, for inspection purposes. It is understood, however, that a measurement system optimized for inspection use would strongly facilitate the actual verification activities.

8.1 BWR assemblies

The experiments done show that partial defect verification of an irradiated BWR assembly, detecting each fuel rod using an array of 10 CdTe detectors, requires about 1 hour of total measurement time.

Experience with the array detector showed also a possible way of reducing the measurement time by increasing the number of detectors in the array. By an array of 20 or 40 detectors, and with the same scanning parameters as used now, the measurement time will decrease proportional to the number of detectors. This means a measurement time of 15-20 minutes for a BWR assembly. Such a measurement head would, however, be heavier and more expensive than the present head.

Further improvement is possible if the objective is not to reveal possible missing of just a single rod (less than 2 % of material) but rather missing of several rods. For research purposes, i.e. to study the potential of the method, a 2 mm sampling distance was used to be able to reconstruct images of high resolution. For practical detection of a missing rod a lower resolution image is enough. Such an image can be achieved by 4 mm sampling. Scanned linear length can also be decreased to about 200 mm. These parameters can be realized by an array of 50 detectors with 4 mm spacing between them. Such a system would no more need linear movement of the detector system. Only rotation of the assembly would be needed. The measurement time could be reduced to 3 - 4 minutes using suitable means of rotating the assembly.

8.2 PWR assemblies

Simulation studies have been made to image also spent PWR assemblies. It is expected that the rod-to-rod burnup distribution for PWR fuel assemblies is more uniform than it is for BWR assemblies. Sensitivity similar to BWR fuel can be achieved also for PWR assemblies but this would require measuring of twice as much views as necessary for BWR fuel. For PWR fuel, the minimum number of views needed is 96. Due to the larger size, the scanned length of about 400 mm is needed. This means an increase of measurement time by a factor of 4 compared to BWR fuel. A large array of detectors is necessary to obtain a practical measurement time.

9 ACKNOWLEDGEMENTS

The Hungarian contribution to this work was supported in part by the Hungarian National Committee for Technical Development and by the International Atomic Energy Agency under Research Contract No. 6549. The authors wish to express their gratitude to the TVO Power Company for the possibility to carry out the measurements and for the help during the measurements. The support of the mechanical workshop and other staff of STUK during the project is highly appreciated.

REFERENCES

/1/ Lévai F, Tikkinen J, Tarvainen M, Arit R. Feasibility studies of computed tomography in partial defect detection of spent BWR fuel. Report STUK-A 97, Finnish Centre for Radiation and Nuclear Safety, Helsinki, Finland, October 1990.

/2/ Lévai F, Dési S, Tarvainen M, Arit R. Detection of missing rods in a spent BWR fuel assembly by computed gamma emission tomography. In: Proceedings of the 32nd INMM Annual Meeting, New Orleans, USA, 1991: 1012-1017.

/3/ Lévai F, Dési S, Tarvainen M, Arit R. Use of an underwater multidetector system for gamma emission tomography of spent fuel assemblies. In: Proceedings of the 15th ESARDA Symposium, Rome, Italy, 1993: 387 - 392.

/4/ Lévai et al. Internal report on the tomographic exercise at TVO, November 1990.

/5/ Lévai et al. Internal report on the tomographic exercise at TVO, June 1991.

/6/ Lévai et al. Internal report on the tomographic exercise at TVO, June 1992.

/7/ Lévai et al. Internal report on the tomographic exercise at TVO, January 1993.

ISBN 951-47-7975-4
ISSN 0785-9325
Painatuskeskus Oy, Pikapaino
Annankatu 44, Helsinki 1993